MINISTRY OF SUPPLY

AERONAUTICAL RESEARCH COUNCIL

CURRENT PAPERS

The Hot-Wire Anemometer for

Turbulence Measurements

Part IV

by

B. Wise, M A., and D. L. Schultz

C.P. No. 276

The Hot-Wire Anemometer for Turbulence Measurements
Part IV
- By -
B. Wise, M.A., and D. L. Schultz,
Oxford University Engineering Laboratory.

O.U.E.L. No.71

Communicated by Prof. A. Thom.

15th April, 1954

SUMMARY

An account is given of some measurements of both turbulence level and spectra at subsonic and supersonic speeds. An investigation of the steady-state heat-loss law over the transonic range is also described.

Contents

1. Introduction

2. Investigation of the Heat-loss Law

    2.1 Measurement of the Equilibrium Resistance R_e.

    2.2 The Heat Loss as a Function of Speed and Temperature.

    2.3 The Heat-loss Law in Dimensionless Form.

    2.4 The Equilibrium Temperature.

    2.5 Further Measurements of $f(m)$.

3. Measurement of Speed

4. Turbulence Measurements

    4.1 Calibration.

    4.2 Turbulence Level with Transonic Liners.

    4.3 Turbulence Level with Plane Walls; Effect of Throat.

5. Spectrum Measurements

    5.1 Wave Analysers.

    5.2 Measurements in Small Tunnel; Effect of Speed Variation.

    5.3 Magnetic Tape Recording.

5.4 Measurements in Larger Tunnel at Subsonic Speeds.

5.5 Measurements in Larger Tunnel at Supersonic Speeds.

~~5.6 Turbulence in Wakes.~~

6. Conclusion

7. Acknowledgements

8. References

------

1. Introduction

It has been shown in earlier papers (Refs. 1,2,3,4) that, by using a radio-frequency constant-resistance technique with tungsten wires, it is possible to measure turbulence at transonic and supersonic speeds with a signal-to-noise ratio which is constant over a wide frequency range. The frequency at which the signal-to-noise ratio begins to deteriorate increases with increasing radio frequency, and is about 20 kc/s if a radio frequency of 100 Mc/s is employed. It has been shown that, by using a negative feedback system employing a mixture of radio-frequency and direct current heating, the response can be made flat up to 50 kc/s, though the signal-to-noise ratio is not thereby improved.

The main purpose of the present paper is to describe measurements which have been made of the turbulence level in high-speed induced-flow wind tunnels at high subsonic and supersonic speeds. A push-pull oscillator using a transmission line at 110 Mc/s was employed, and this gave a bandwidth of about 20 kc/s. Since it was found by spectrum analysis that the bulk of the turbulent energy usually fell below 5 kc/s, this bandwidth proved more than adequate, and no use has been made of the wider bandwidth which can be obtained in the more complex system using negative feedback and mixed heating currents. This latter would no doubt prove useful in any experimental work on turbulence in boundary layers or wakes, where much high frequencies have been observed (Refs. 5,6).

As a preliminary to the work on turbulence a considerable amount of experimental work on the static heat-loss law for the wire was undertaken.

It was found that the temperature of the wire when it is not electrically heated, T_e, lies between the temperature of the stream T and the stagnation temperature T_s, and the relation is a linear one above about $M = 0.7$ (see Section 2.4). When the wire is electrically heated, and its temperature T_w is such that $T_w - T_0 \ll T_s$, the heat loss W is proportional to $T_w - T_e$, so that $\dfrac{W}{T_w - T_e}$ is constant at a fixed speed. At higher wire temperatures, $\dfrac{W}{T_w - T_e}$ is a function of temperature and may be expressed approximately in the form

$$A + B\ \frac{T_w - T_e}{T_e} + C\left(\frac{T_w - T_e}{T_e}\right)^2 \qquad \text{(Section 2.3)}$$

At low velocities it is well known that the heat loss is given by King's equation and is proportional to $a + b\sqrt{u}$. At somewhat higher speeds W is proportional to (mass-flow)$^{\frac{1}{2}}$, i.e., $\sqrt{\rho}\,u$. Above a Mach number of about 0.4, however, $\dfrac{W}{\sqrt{\rho}\,u}$ falls, and W reaches a maximum at about $M = 0.8$,

instead/

instead of at $M = 1$, as it would if $\dfrac{W}{\sqrt{\rho\,u}}$ remained constant. The ratio $\dfrac{W}{\sqrt{\rho\,u}}$ continued to fall, up to the highest Mach number used, 1.36. In the range $0.32 < M < 1.32$ the variation of $\dfrac{W}{\sqrt{\rho\,u}}$ can be empirically described by a rational function $\dfrac{a + bM}{c + M}$.

Combining the results, (Section 2.3),

$$W \propto \sqrt{\rho\,u}\;\frac{a + bM}{c + M}\;(T_w - T_e)\left\{A + B\left(\frac{T_w - T_e}{T_e}\right) + C\left(\frac{T_w - T_e}{T_e}\right)^2\right\}.$$

2. Investigation of the Heat-loss Law

In establishing a heat-loss law a prime necessity is a really accurate method of measuring the resistance of the wire and its power input. The voltage across the wire was measured by means of a potentiometer, and the current by measuring the voltage it produced across a standard resistance. The resistance of the wire was either obtained from the voltage and current, or directly from a bridge circuit using standard resistances. The order of accuracy when the larger of the two tunnels was in use was usually 0.01%, except at high subsonic speeds where conditions were more subject to fluctuation. The accuracy naturally decreases as the magnitude of voltage and current are decreased, so that measurement of the equilibrium resistance R_e, i.e., the resistance with no electrical heating, presents a real problem. This is considered in the next Section.

When it has been shown that the heat loss at a fixed speed is approximately proportional to $R - R_e$ and more accurately to $(R - R_e) + \beta_1(R - R_e)^2 + \beta_2(R - R_e)^3$, the next step is to investigate its dependence on the mass-flow. The first essential is to estimate the actual speed of the air flowing past the wire, and this can only be done by inference from a measurement made with a static pressure probe in the same position. It has proved necessary to make the shape of this probe as nearly as possible the same as that of the wire probe. Results are given in Section 3.

If the approximate relation for the heat loss is expressed as follows:

$$W = f(m)\,(R - R_e),$$

the problem is to measure $f(m)$ for various mass-flows. The most obvious way is to plot a graph of W against R; this should be a straight line whose slope gives $f(m)$. It has proved unexpectedly difficult to do this accurately, but analysis of one set of readings (Section 2.2) gives results which are in agreement with those obtained by Santon in 1933 (Ref.7); these latter are referred to on p.85 of Ref.8.

2.1 Measurement of the Equilibrium Resistance R_e

When the electrical power input to the wire, W, is small, we may write

$$W = f(m)\,(R - R_e),$$

where $f(m)$ is a constant at a given speed, and the problem is to find R_e.

The first method used was to plot W against R and extrapolate to $W = 0$. At first a resistance bridge method was used so that readings could be obtained at equidistant values of R. Later, the bridge was omitted, the wire resistance being deduced from measurements of the voltage and current, obtained by means of a potentiometer and standard resistance.

The/

The first system had an advantage over the second, in that two microammeters were used, one indicating the balance of the bridge and the other the balance of the potentiometer, and both these could be observed at the same time. This means that, if readings are taken when both meters indicate zero (the readings fluctuate with time owing to variations in tunnel conditions), one can be sure that the correct voltage has been found corresponding to the resistance set up in the bridge.

In the second system, where voltage and current are measured one after the other, tunnel conditions may change slightly meanwhile, and this introduces some inaccuracy. In practice, however, this second system was found to be more convenient.

The following table gives a typical set of readings for finding R_e; they were taken with a wire 0.000275 inches in diameter at a Mach number of 0.9. The currents, which were inferred from the voltage they produced across 10 ohms, were arranged to be approximately $1, \sqrt{2}, \sqrt{3}, \sqrt{4}$ and $\sqrt{5}$ times 10 mA. The power intervals are then approximately equal.

Current in mA	Voltage in mV	Resistance in ohms	Power in microwatts	Voltage from formula	Error
9.937	12.22	1.2297	121.4	12.22	0
14.098	17.36	1.2314	244.7	17.36	0
17.334	21.37	1.2328	370.4	21.37	0
20.023	24.71	1.2341	494.8	24.68	-0.03
22.507	27.80	1.2352	625.7	27.81	0.01

By the method of least squares (see for example Ref.9, Chap.IX), the following relation between power and resistance can now be found:

$$W = 91.30 \ (R - 1.2286) \ \text{milliwatts.}$$

The relation between voltage in mV and current in mA is then

$$V = \frac{0.11217 \ I}{0.09130 - I^2} \qquad V = \frac{112.17 \ I}{91,300 - I^2} .$$

As a check on the experimental error we calculate the voltage from this formula for each current used, and obtain the last two columns in the above table. The agreement is good, so the value obtained for R_e, i.e., 1.2286 ohms, may be relied on.

A second method is based on an analysis of the voltage-current relationship, as follows:

From

$$VI = f(m) \left\{ \frac{V}{I} - R_e \right\}$$

we can write

$$V = R_e I + \frac{VI^2}{f(m)}$$

$$V \simeq R_e I + \frac{R_e I^3}{f(m)} .$$

The voltage is measured for a set of equally-spaced currents, and a least-squares analysis done on the assumption $V = R_e I + \lambda I^3$.

The following table gives a typical set of results from which the following equation was found:

$$V = 1.6450\,I + 0.0018222\left(\frac{I}{3}\right)^3,$$

with V in mV and I in mA.

Current in mA	Voltage in mV	Voltage from formula	Error
3	4.93	4.94	0.01
6	9.88	9.88	0
9	14.85	14.85	0
12	19.86	19.86	0
15	24.91	24.90	-0.01
18	30.00	30.00	0
21	35.17	35.17	0

A third method of finding R_e is based on a re-arrangement of the basic formula as follows:

From
$$VI = f(m)\left\{\frac{V}{I} - R_e\right\}$$

we have, dividing by R,
$$I^3 = f(m)\left\{1 - R_e\frac{I}{V}\right\}.$$

Thus at low power levels there is a linear relation between the conductance and I^2. The current was set by means of the potentiometer at a series of values which gave equidistant values of I^2, and the voltage then measured. A least-squares analysis is here more easily carried out than in either of the two other methods as the relationship is linear, and the values of one variable are equally spaced. For this reason this last was the method most often used.

The following table gives a set of readings for a wire at $M = 0.9$.

I^2 in (mA)^2	V in mV	$\frac{I}{V}$ in millimhos	$\frac{I}{V}$ from formula	Error in $\frac{I}{V}$	V from formula	Error in V
800	34.92	809.97	810.02	-0.05	34.92	0
1200	42.96	806.38	806.38	0	42.96	0
1600	49.83	802.73	802.74	-0.01	49.83	0
2000	55.95	799.32	799.10	0.22	55.97	-0.02
2400	61.60	795.29	795.45	-0.16	61.59	0.01

The/

The formula obtained by least squares analysis is

$$\frac{I}{V} = 817.31 - 0.009105 \, I^2 \text{ millimhos} , \qquad \ldots (1)$$

where I is in mA.

The difference between the values of $\frac{I}{V}$ and V given by this formula and the experimental ones are tabulated above.

2.2 The Heat Loss as a Function of Speed and Temperature

When the temperature of the wire is maintained at a constant level much higher than T_e, say $1.5 \, T_e$, the variations in T_e which occur as the speed is varied have little effect, and the input power provides a measure of the heat loss directly as a function of speed. This is what happens with the oscillator circuit used for turbulence measurements, which keeps the wire resistance R constant at a value considerably in excess of the cold resistance R_e. If we anticipate an empirical formula for the power input W, established later, $W = f(m) [R - R_e + \beta_1 (R - R_c)^2 + \beta_2 (R - R_c)^3]$, we see that the coefficient $f(m)$ will be directly proportional to the oscillator voltage squared.

Measurements were made using an oscillator with a wire in a small induced-flow wind tunnel and a typical graph of the voltage is shown in Fig.1. It will be seen that a maximum is reached at a Mach number of 0.75.

To investigate this phenomenon more accurately, it was decided to make D.C. measurements with a resistance bridge and potentiometer. The power input required to maintain the resistance constant at five different levels was measured at eleven Mach numbers. In addition, the equilibrium resistance at each Mach number was estimated from five measurements at low power, using the first method described in Section 2.1. This entailed taking altogether 110 readings with the same wire. When the equilibrium resistances were plotted against the tunnel pressure, it was found that they were subject to considerable scatter, so the results were smoothed by the orthogonal polynomial method (see Ref.9). Using the smoothed values of R_e, the powers were computed by interpolation for values of $(R - R_e)$ equal to 0.9, 0.7, 0.5, 0.3 and 0.1 ohms, at each Mach number.

Assuming that the heat loss can be expressed in the form:

$$W = f(m) \cdot g(R - R_e)$$

and two measurements are made at the same speed,

$$W_1 = f(m)g(R_1 - R_e)$$
$$W_2 = f(m)g(R_2 - R_e),$$

it follows that $\frac{W_1}{W_2}$ should be the same at all speeds. This power ratio was computed with $R_1 = 0.7$ ohms, and $R_2 = 0.9$ ohms, and the result averaged over the whole range of speeds. The deviations of the ratios from this average appeared random, and this was also the case when R_1 was 0.5 and 0.3 ohms, R_2 being 0.9 ohms in each case. The power ratio with $R_1 = 0.1$ ohms and $R_2 = 0.9$ ohms showed a more systematic deviation from the mean, which is unexplained. The means of these power ratios were used to find the function $g(R - R_e)$, by means of a least-squares approximation, the result being:

$$g(R - R_e) \propto (R - R_e) - 0.452 (R - R_e)^2 + 0.204 (R - R_e)^3.$$

The/

The values of $f(m)$ at each speed were now obtained by fitting the experimental results to the equation:

$$W = f(m) \left[(R - R_e) - 0.452 (R - R_0)^2 + 0.204 (R - R_e)^3 \right],$$

again by the method of least squares.

The result is plotted as curve (1) in Fig. 2. It will be seen that a maximum occurs at $M = 0.8$, which is similar to the results obtained with the radio-frequency oscillator. As previously remarked, $f(m)$ could be expected to be proportional to $\sqrt{\rho u}$, so an empirical formula to fit the observations has been based on the ratio $\dfrac{f(m)}{\sqrt{\rho u}}$, which is plotted in Fig. 3.

Since this ratio falls with increasing Mach number it may be expressed in the form $y = \dfrac{a + bM}{c + M}$, so that at low values of M it is equal to $\dfrac{a}{c}$ and at high Mach numbers it is equal to b. By minimising $\Sigma(yc + yM - a - bM)^2$ we find

$$
\begin{bmatrix}
\Sigma 1 & \Sigma x & \Sigma y \\
\Sigma x & \Sigma x & \Sigma xy \\
\Sigma y & \Sigma xy & \Sigma y
\end{bmatrix}
\begin{bmatrix}
a \\
b \\
-c
\end{bmatrix}
=
\begin{bmatrix}
\Sigma xy \\
\Sigma x^2 y \\
\Sigma xy^2
\end{bmatrix}
$$

Solving for a, b and c, we find

$$f(m) = 0.14325 \sqrt{\frac{\rho}{\rho_s} \frac{U}{a_s} \frac{4.82 + 7.55 M}{2.67 + 10 M}} \quad (\text{amps})^2$$

where ρ_s is the density under stagnation conditions and a_s is the sonic speed under sonic conditions $\left(\dfrac{\rho}{s} \text{ and } \dfrac{u}{a_s} \text{ are tabulated in Ref. 12} \right)$. Values given by this function are indicated by crosses on Fig. 2, from which it will be seen that the fit is good.

It is useful to have such an empirical formula to fit the observations so that it can be differentiated at any Mach number to find the fluctuation sensitivity.

Another possibility for an empirical formula is to take

$$f(m) \propto \sqrt{\rho u} \left(\frac{T}{T_s} \right)^{\tau}$$

which will approximate to $\sqrt{\rho u}$ at low speeds. It is found that τ is 0.78 for the best fit, which, however, is very poor. The result is shown as curve (2) in Fig. 4, curve (1) being the experimental one.

This formula may also be expressed as

$$M^{0.5} \left(\frac{T}{T_s} \right)^{2.38}$$

In/

In general, we may take:

$$f(m) = k(M)^{\eta} \left(\frac{T}{T_s}\right)^{\zeta} \qquad \ldots (2)$$

and compute k, η and ζ to give the best fit (see Ref. 9 p.247). Then it is found that $\eta = 0.211$ and $\zeta = 1.025$. The result is given as curve (3) on Fig. 4; the fit is still poor.

It can be shown that if the heat loss is given by (2) the maximum will occur at $M = 0.8$ if $\eta = 0.227\zeta$, and this is roughly satisfied in both the above cases.

Another possible formula is

$$f(m) \sqrt{\rho u} \ M^{\sigma} .$$

This gives a maximum at 0.8 if $\sigma = -0.16$, and, when arranged to have the same maximum value as the experimental curve, this gives points shown by $\triangle$ on Fig. 4.

We may remark here that, since the relevant viscosity may be supposed to be approximately that corresponding to stagnation conditions, μ_s, ρu is proportional to the Reynolds number, and

$$\frac{\rho u}{\rho_s a_s} = \frac{R_e \mu_s}{\rho_s a_s d}$$

where d is the wire diameter.

Taking $\mu_s = 0.374 \times 10^{-6}$ slugs/ft sec., $\rho_s = 0.00238$ slugs/cu ft, $a_s = 1023$ ft/sec, $d = 0.000275$ inches, we find

$$\frac{\rho u}{\rho_s a_s} = 6.70 \times 10^{-3} R_e$$

and

$$\sqrt{\frac{\rho}{\rho_s} \frac{u}{a_s}} = 0.0819 \sqrt{R_e} .$$

Thus

$$f(m) = \sqrt{R_e} \ \frac{5.66 + 8.85 M}{2.67 + 10 M} \ 10^{-3} \ (\text{amps})^2 .$$

2.3 The Heat Loss Law in Dimensionless Form

From the previous Section, we have

$$W = f(m) \{(R - R_e) - 0.452 (R - R_e)^2 + 0.204 (R - R_e)^3\} (mA)^2 .$$

Taking $(R - R_e) = \alpha (T_w - T_e)$, where $\alpha = 51 \times 10^{-4}$ ohms/$^{\circ}$C, this may be expressed as follows:

$$\frac{W}{T_w - T_e} = f(m) \ 51 \times 10^{-4} (1 - 0.452 (R - R_e) + 0.204 (R - R_e)^2) .$$

If, further, an average value for T_e of 280°K is taken, the terms $(R - R_e)$ and $(R - R_e)^2$ may be expressed approximately in dimensionless form by writing

$$(R - R_e) = 51 \times 10^{-4} \ 280 . \ \frac{T_w - T_e}{T_e} = 1.428 \ \frac{T_w - T_e}{T_e} .$$

Then/

Then $\dfrac{W}{T_W - T_e} = f(m)\ 51 \times 10^{-4} \left[1 - 0.645 \left(\dfrac{T_W - T_e}{T_e}\right) + 0.416 \left(\dfrac{T_W - T_e}{T_e}\right)^2\right].$

The Nusselt number is defined to be

$$\frac{W}{(T_W - T_e)\ \pi\ L\ k_f}$$

where k_f is the conductivity of the air, and L is the length of the wire.

Taking the relevant conductivity to be approximately the same as under stagnation conditions, i.e., 5.22×10^{-5} cals/sq cm/cm/sec/°C, and $L = 0.10$ cm, we get

$$W = 6.85 \times 10^{-5}\ (T_W - T_e)\ \text{Nu watts}.$$

Writing $f(m)$ from the previous Section, we now have

$$\text{Nu} = \frac{1}{6.85 \times 10^{-5}}\ \sqrt{R_e}\ \frac{5.66 + 8.85M}{2.67 + 10M}\ 10^{-2} \cdot 51 \cdot 10^{-4} \left\{1 - 0.645\left(\frac{T_W - T_e}{T_e}\right) + 0.416\left(\frac{T_W - T_e}{T_e}\right)^2\right\}$$

$$= \sqrt{R_e}\ \frac{4.21 + 6.59M}{2.67 + 10M}\left\{1 - 0.645\left(\frac{T_W - T_e}{T_e}\right) + 0.416\left(\frac{T_W - T_e}{T_e}\right)^2\right\}.$$

A curve showing how Nu varies with $\sqrt{R_e}$ over the range $0.3 < M < 1.4$ for $\dfrac{T_W - T_e}{T_W}$ small, is shown in Fig. 5. With increasing T_W the Nusselt number increases by the factor contained in the above formula. A similar curve was obtained by Santon (Ref. 7). The results may be compared with those given in Refs. 10 and 11.

2.4 The Equilibrium Temperature

From the results given in Section 2.2 we may investigate the relation of the equilibrium temperature of the wire T_e to the stream temperature T and the stagnation temperature T_s. The equilibrium temperature at any speed can be found from the equilibrium resistance R_e at that speed and the resistance measured at zero speed, R_s, where the temperature is the same as the stagnation temperature:

$$(T_s - T_e) = \frac{1}{\alpha}\ (R_s - R_e), \quad \alpha = 51 \times 10^{-4}.$$

From the smoothed curve of R_e against pressure, values of R_e were read off at pressures corresponding to various values of $\dfrac{T}{T_s}$ and the resulting relation between $\dfrac{T_s - T_e}{T_s}$ and $\dfrac{T_s - T}{T_s}$ is shown in Fig. 6. It will be seen that the relation is linear when $\dfrac{T_s - T}{T_s} > 0.08$, i.e., $M > 0.65$; the equation here is:

$$\left(\frac{T_s - T_e}{T_s}\right) \cdot 100 = 1.26 + 0.19455 \left(\frac{T_s - T}{T_s}\right) \cdot 100.$$

The shape of the curve below this linear range indicates that T_e is more dependent on T at lower speeds than at higher.

2.5/

4.3 **Turbulence Level with Plane Walls. Effect of Second Throat**

Corresponding measurements of u'/U were made in the 9" × 3" tunnel fitted with plane walls, and the results are shown in Fig. 15. The level is seen to remain constant at a much lower value, about 0.12%, up to 600 ft/sec, but above this speed there is a rapid and large increase. It was thought likely that acoustic waves generated by the injection mechanism could account for this type of variation in turbulence level, and a second throat was installed between the working section and the injector slots and designed to choke at a Mach number of 0.6. Below choking speed it will be observed from Fig. 15 that the level is increased, at least above 300 ft/sec, and this is not unexpected since the throat was made of two wedges with sharp downstream edges, and it is not unreasonable to expect that below their choking point they will generate sound waves themselves in the downstream region of shear.

At choking point, however, the level in the working section is reduced from 0.25 to 0.16% u'/U. Apparently 36% of the turbulence in the working section is accounted for by disturbances proceeding upstream. The calibration curve and fluctuation sensitivity are shown in Fig. 15 also. Screens C, D and E were in the contraction; with a more carefully designed throat it would be expected that the turbulence before choking would not be so much increased as is the case with the throat used. Similar results were obtained with throats designed to choke at higher speeds, the "choked" condition giving a working section turbulence level of about 0.15 to 0.18%.

It is concluded therefore that the turbulence level in the plane-walled tunnel is lower than that in the same tunnel fitted with transonic liners up to about 600 ft/sec. Above this the latter tunnel produces a lower level of turbulence except when second throats are installed.

5. **Spectrum Measurements**

Little information was available on the expected spectral density of turbulence in high speed flows, although theoretical considerations lead to a curve rising from zero frequency and decaying again. It has been shown (Ref. 6) by high-speed schlieren photography that in wakes at high airspeeds frequencies of the order of some hundreds of kilocycles would occur, but no measurements had been made at the time in the free streams of supersonic or even high speed subsonic tunnels.

The use of an electrical wave analyser has become a standard technique for examining the spectra of random fluctuations, and the criteria for such instruments are discussed in Section 5.1.

5.1 **Wave Analysers**

Preliminary investigation of the spectrum of turbulence in a low speed jet had shown that the energy level over narrow bandwidths was subject to wide variations and some averaging device would be essential at the output of the filter network. It was further decided that the bandwidth available from crystal filter type analysers was too narrow, and circuits which would permit a constant bandwidth of about 50 c/s to be obtained were investigated. Twin-T negative feedback loops and regenerative amplifiers were constructed, but failed to produce the required narrow bandwidth, suffering in addition from too low an attenuation several kilocycles off tune. This latter feature was thought to be desirable if low energy levels at high frequencies were to be discriminated from larger levels at lower frequencies.

An analyser operating on the conventional heterodyne principle was constructed which had an intermediate frequency amplifier with a response level from 0.5 to 20 c/s. A block diagram is shown in Fig. 16. The local oscillator is tuned to the centre frequency f it is desired to select, then all frequencies between $(f - 20)$ and $(f + 20)$ c/s are passed into the low frequency amplifier and recorded on the vacuo junction. It was possible to vary the pass band of

this/

this amplifier by means of negative feedback, and thus adjust the selectivity of the whole unit. A pre-amplifier was fitted with high attenuation in the range 0.5 to 100 c/s to prevent low-frequency breakthrough, but in practice it was found that the energy level of low frequency turbulence was still causing breakthrough, and this anslyser was abandoned in favour of a commercial heterodyne analyser with a crystal filter. The filter unit was modified to give the response shown in Fig. 17, the original response being shown also. The bandwidth 10 dB down has been extended to 10 c/s and although this was still well below the required 50 c/s it proved reasonably satisfactory.

5.2 Turbulence Spectra in 2 Inch Tunnel: Effect of Speed Variation

Using the modified wave analyser described in the previous section, the flow in the working section of this tunnel fitted with a transonic liner was examined. It was found that reproducible spectra could be drawn and that there was evidence of large peaks at discrete frequencies. A typical spectrum at M = 0.89 is shown in Fig. 18 where two peaks at 2,900 and 4,400 c/s will be observed. It was thought that wire vibration could be a possible source of such sharply defined peaks, since mechanical vibrations are typically pure and exhibit no harmonics. Several changes were made in the wire mounting and tension, but no corresponding changes were observed in the spectrum, and it is therefore concluded that such peaks occur in the spectrum. Vibration of the tunnel walls would typically occur at a much lower frequency. Resonance in the air column may be one possible explanation of the behaviour, but no evidence can be presented in support of this at present. The peak frequencies varied with mean air velocity, an increase in velocity causing an increase in frequency, although below about M = 0.5 the peaks became much less evident. The output at 5 kc/s is shown in Fig. 19 plotted against air speed. It will be seen that as M = 0.90 is approached the output begins to rise, due to the approach of the second peak in Fig. 18, the frequency of which is rising with speed.

5.3 Magnetic Tape Recording

The time taken to record a complete spectrum was found to be a serious disadvantage in the larger tunnel, whose running time at supersonic speeds was limited, and a tape recording technique was used to reduce this. Such a method also enables a more detailed spectrum to be drawn, since the tape may be cut into lengths of about 18 inches and replayed with the ends joined to form closed loops. The output is then examined in the usual way by means of the wave analyser, and any portion may be resolved in as much detail as is required. With such a short loop length the output from the wave analyser filter remains very steady, or at worst moves in a regular manner between two fixed limits. The tape recording equipment was of restricted bandwidth, uniform from about 200 c/s to 8 kc/s, so that the results presented cannot be regarded as accurate, but they illustrate the value of such a technique.

5.4 Turbulence Spectra in 9" × 3" Tunnel at Subsonic Speeds

A typical spectrum recorded on a tape loop corresponding to 1.3 seconds of tunnel running time is shown in Fig. 20. The spectral density is seen to rise from zero to about 3 kc/s and then decay. The mean tunnel speed was M = 0.36. It was observed that the total turbulence was higher when the fine control valve was used in the inlet to the injector slots, and spectra for both the coarse and fine control valve conditions are shown in Fig. 20. The scales for these two curves are not the same and in fact the total level of turbulence in the fine-control case was 1.23 times that in the other. Thus for a true comparison the area under the "fine" curve ought to be arranged to be 1.23 times the other. The total turbulence was found to vary with time and the recording technique enabled a more accurate spectrum to be drawn under these conditions. A spectrum taken with the tunnel running continuously is shown for comparison in Fig. 21, the minimum and maximum readings during an interval of 30 seconds being plotted. The total time taken was thus 8.5 minutes.

Comparison/

. Comparison of Figs. 20 and 21 shows that there is a large discrepancy between the spectrum observed over a time interval of 1.3 seconds and 8.5 minutes, which cannot be accounted for in the recording technique, at least between 200 c/s and 8 kc/s. Apparently there is a differing intermittency rate at each frequency, and to obtain a more complete picture many more recorded examples would have to be analysed and an average taken of the results.

When plotting a spectrum with the tunnel running continuously, it was observed that the output of the analyser sometimes fell to a much lower level than the average and would remain there before rising again. Such violent excursions are not always observed in the half-minute intervals used in obtaining Fig. 21.

In Fig. 22 is shown the spectrum obtained at a much higher subsonic speed, M = 0.99, in the 9" × 3" tunnel. The points plotted are the means obtained in half-minute periods as in Fig. 21. A sharp decay in energy level will be noticed, although above about 8 kc/s the level remains fairly constant.

5.5 Turbulence Spectra in Free Stream at Supersonic Speeds

The spectrum in the test diamond of the 9" × 3" tunnel at M = 1.8 was recorded and is plotted in Fig. 23. Screens C, D, and E and the turbulence grid were in the contraction. The presence of distinct peaks will be noted at quite low frequencies although it must also be remembered that the higher frequencies are not accurately recorded. Nevertheless, the spectrum shows a concentration of energy below 8 kc/s. When the spectrum in a similar flow was studied with the tunnel running continuously (Fig. 24) it was difficult to locate these peaks due to their narrow bandwidth, the high selectivity of the analyser and the random nature of the signal. It was observed that below 2 kc/s the two spectra were somewhat different, that recorded on the tape showing a decay while the other indicated increasing energy.

The output of the vacuo-junction at low frequencies is subject to wide variations which are almost periodic in character. These may be due to fluctuations in the mean tunnel speed, which would not necessarily occur during the 1.5 second interval recorded on the tape.

6. Conclusion

It has been shown that the radio-frequency constant-resistance technique is suitable for the measurement both of turbulence levels and also of turbulence spectra at any Mach number up to 1.8. There is no reason to suppose that any difficulty would be experienced at higher Mach numbers.

The/

The heat-loss law at high subsonic speeds is a complicated one so that the separation of mass-flow, temperature and Mach number effects will be difficult at these speeds.

7. Acknowledgments

The work described here was done at the National Physical Laboratory; we are grateful to the Director for the facilities afforded, and to the staff of the High Speed Aerodynamics Division for their generous assistance.

We would also like to express our gratitude to Professor A. Thom for his interest and encouragement throughout the course of this work.

References

No.	Author(s)	Title
1	B. Wise	The hot-wire anemometer for turbulence measurements, Part I. O.U.E.L. No.52. Presented by Prof. A. Thom. C.P. 273. February, 1951 10
2	B. Wise and D. R. Stewart	The hot-wire anemometer for turbulence measurements, Part II. O.U.E.L. No.54. Presented by Prof. A. Thom. C.P. 274. September, 1951.
3	B. Wise and D. L. Schultz	The hot-wire anemometer for turbulence measurements, Part III. O.U.E.L. No.69. Communicated by Prof. A. Thom. C.P. 275. March, 1954.
4	D. L. Schultz	The design and construction of hot-wire anemometers for high-speed flows. O.U.E.L. No.68. Communicated by Prof. A. Thom. A.R.C.16,635. March, 1954.
5	L. S. G. Kovásznay	Turbulence in supersonic flow: annual meeting of Inst. Aero. Sci. Jan. 1953.
6	L. S. G. Kovásznay	Technique for the optical measurement of turbulence in high speed flow. Heat Transfer and Fluid Mechanics Inst. 1949. Berkeley, California.
7	M. L. Santon	Quelques résultats obtenus avec une soufflerie supersonique. Comptes Rendus, Jan.-June 1933.
8	E. G. Richardson	Dynamics of real fluids. Arnold & Co., 1950.
9	W. E. Milne	Numerical calculus. Princeton University Press, 1949.
10	H. H. Lowell	The design and application of hot-wire anemometers for steady state measurements at transonic and supersonic airspeeds. N.A.C.A. T.N.2117.

No.	Author(s)	Title
11	L. S. G. Kovásznay and S. Törmarck	Heat loss of wires in supersonic flow. Bumblebee Report No.127. Johns Hopkins University.
12	Tables	Compressible airflow. Clarendon Press, Oxford.
13	D. W. Holder and R. J. North	The 9" × 3" N.P.L. induced-flow high-speed wind tunnel. A.R.C.12,387 - T.P.285. 1st June, 1949.
14	Bond	Probability and random error. Arnold 1932.

JDK.

FIG 1

Calibration of oscillator
2" tunnel

FIG 2

f(m) as function of M.

o Experimental points, smoothed.

+ Rational function,

$$\frac{f(m)}{\sqrt{\rho u}} = \frac{4\cdot82 + 7\cdot55\,M}{2\cdot67 + 10\,M}$$

FIG 3

$\dfrac{f(m)}{\sqrt{\rho}\,u}$ as a function of Mach $N^{\underline{o}}$

o   Experimental $\dfrac{f(m)}{\sqrt{\rho}\,u}$

+ $\dfrac{f(m)}{\sqrt{\rho}\,u} = \dfrac{7\cdot82 + 7\cdot55\,M}{2\cdot67 + 10\,M}$

$\dfrac{f(m)}{\sqrt{\rho}\,u}$

M ⟶

FIG 4

f (m) as a function of Mach No

f (m), (mA)²

M →

Legend

(1) ○ Experimental f (m)

(2) ✕ f (m) = $\dfrac{k_1 \, M^{05}}{(1+0\,2M^2)^{2\,28}}$

(3) + f (m) = $k_2 \, \dfrac{M\,0\,211}{(1+0\,2M^2)^{1\,025}}$

(4) △ f(m) = $\sqrt{\rho u} \; M^{-016}$
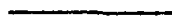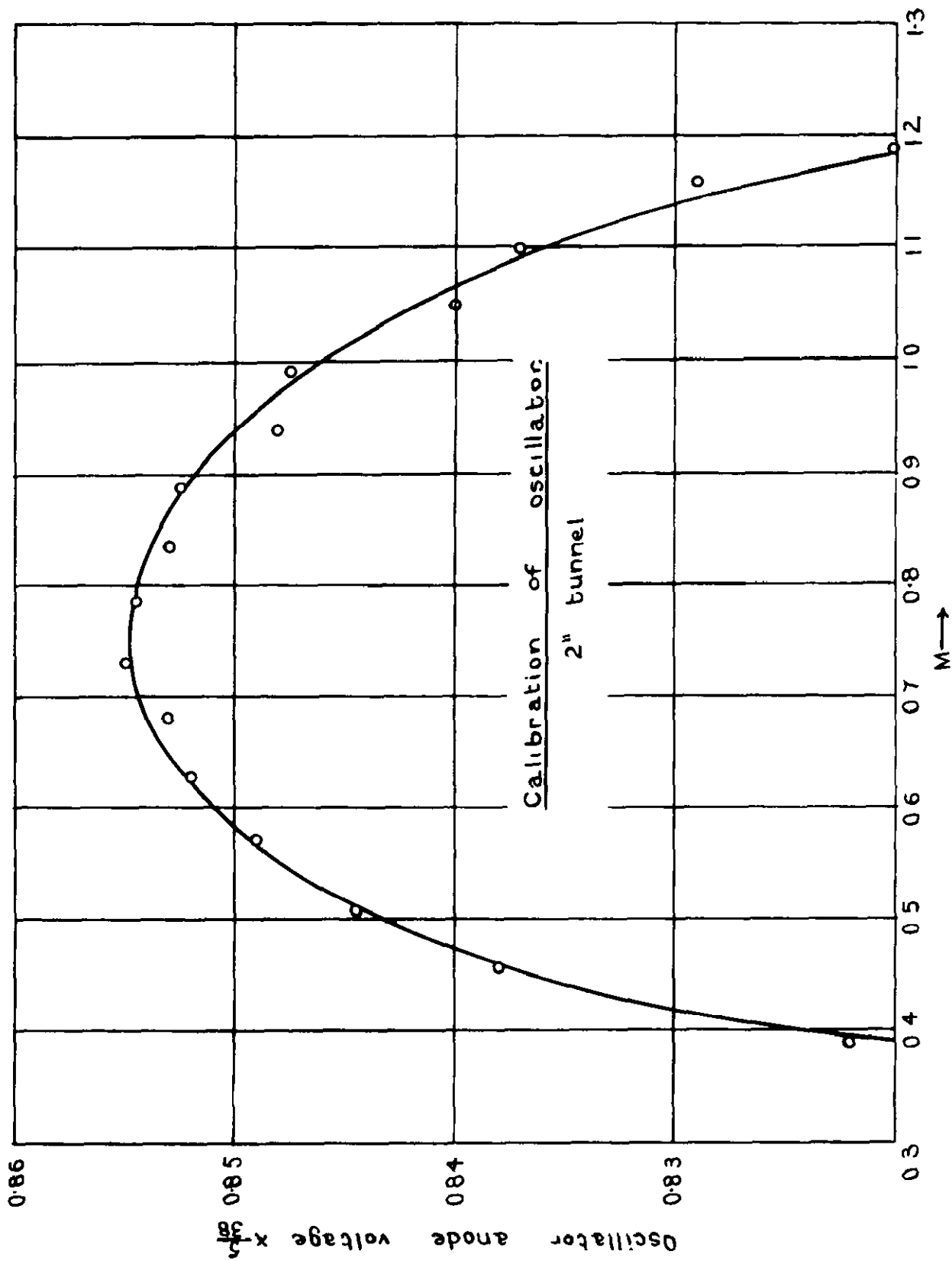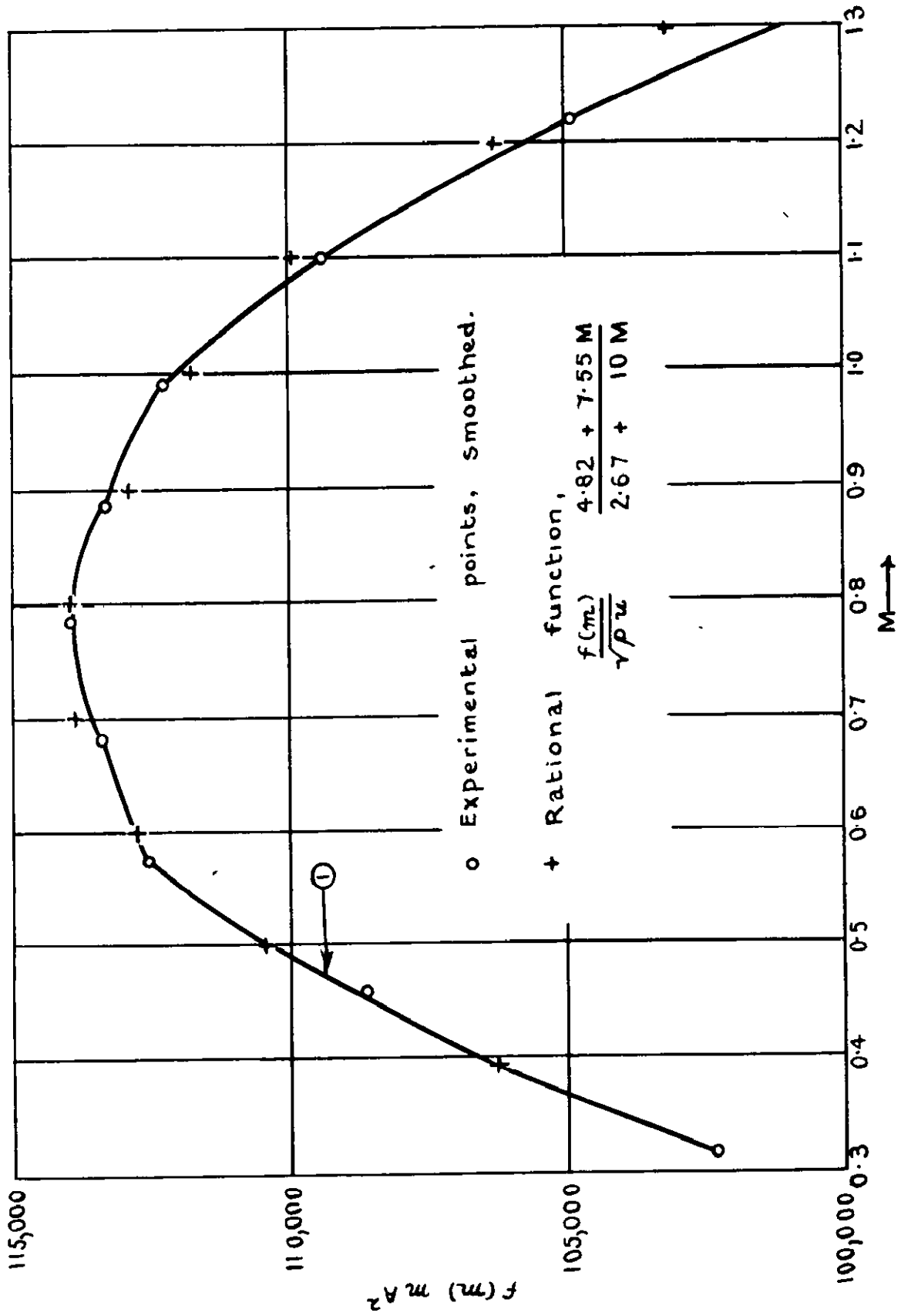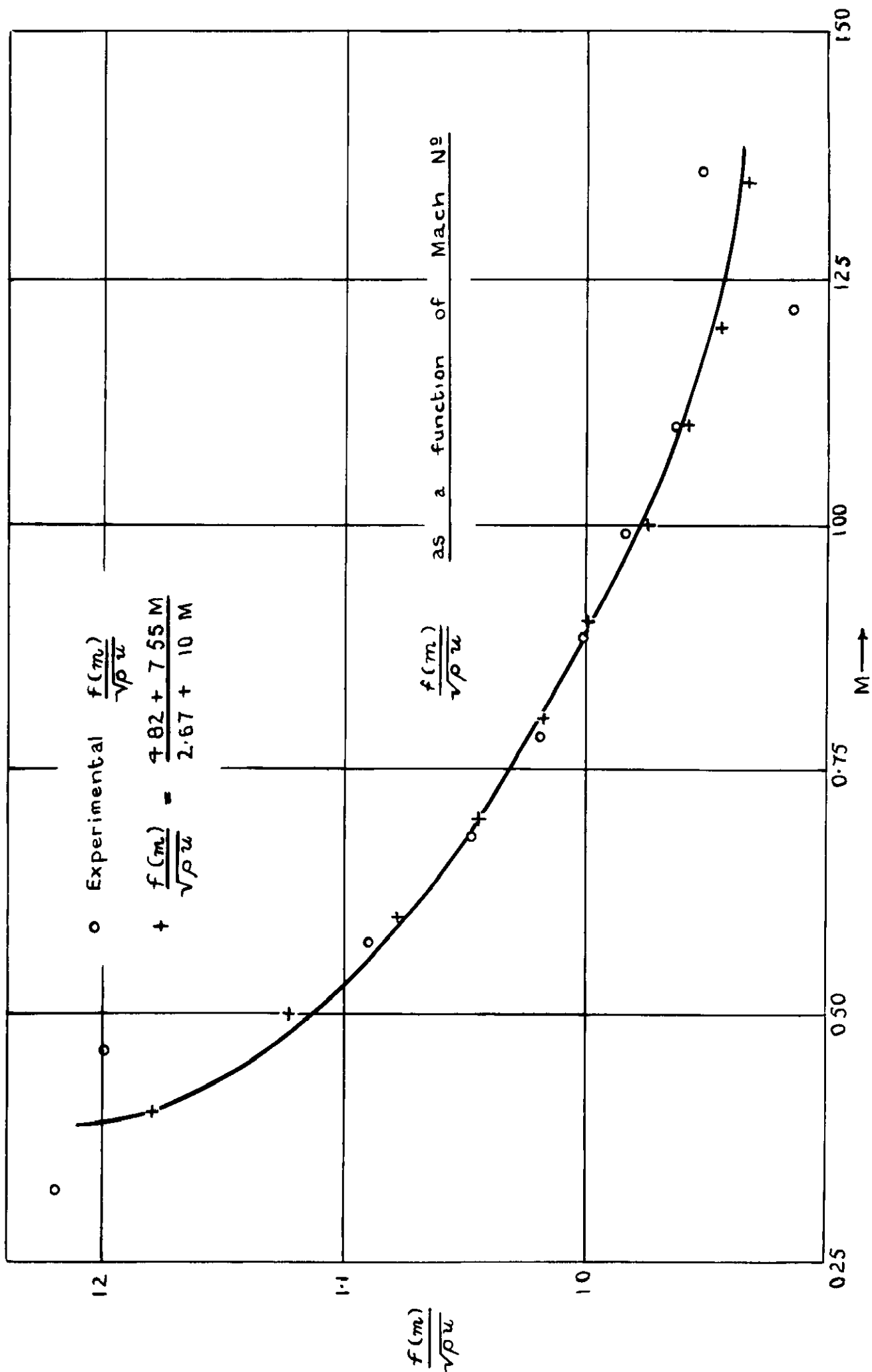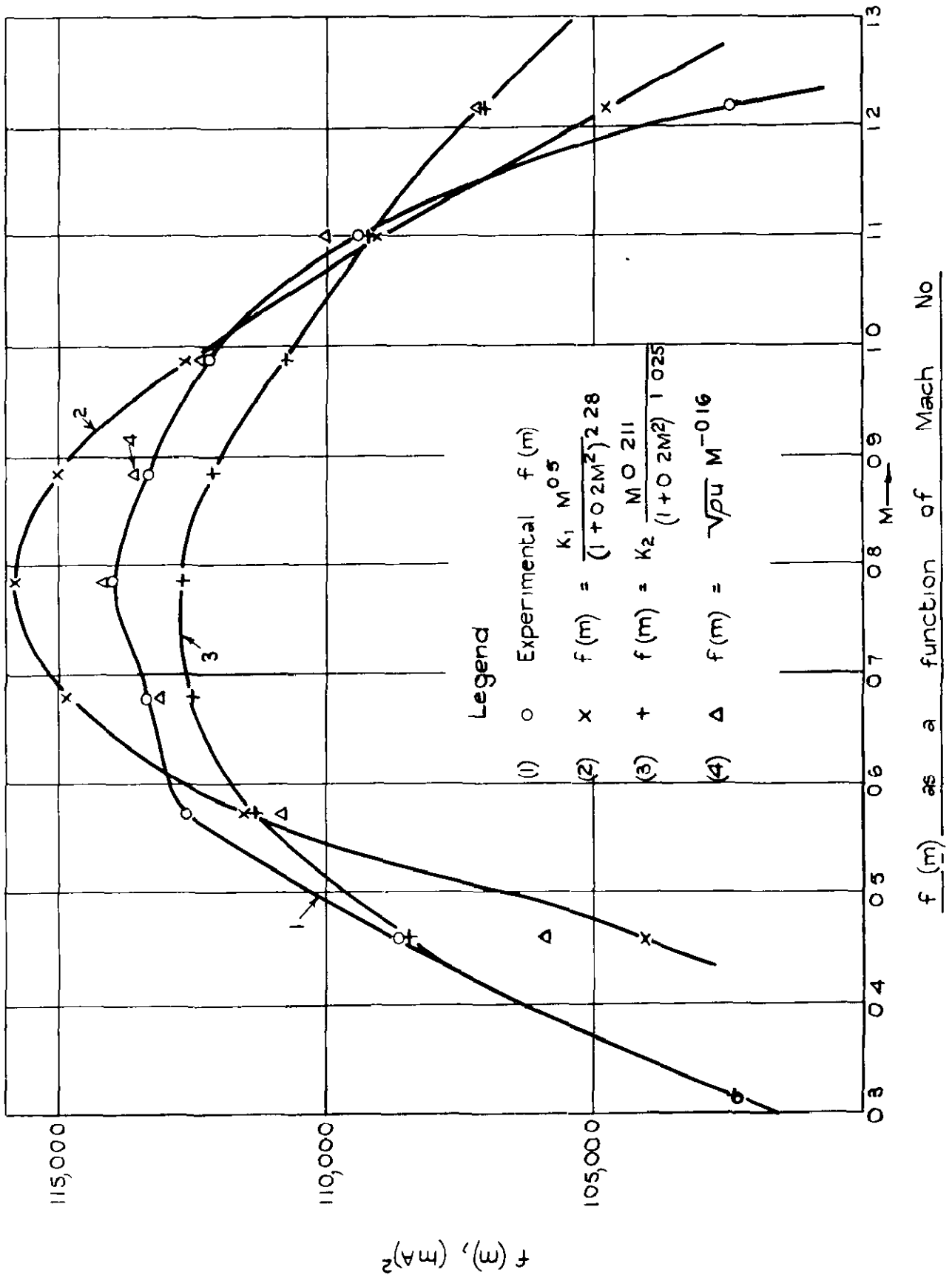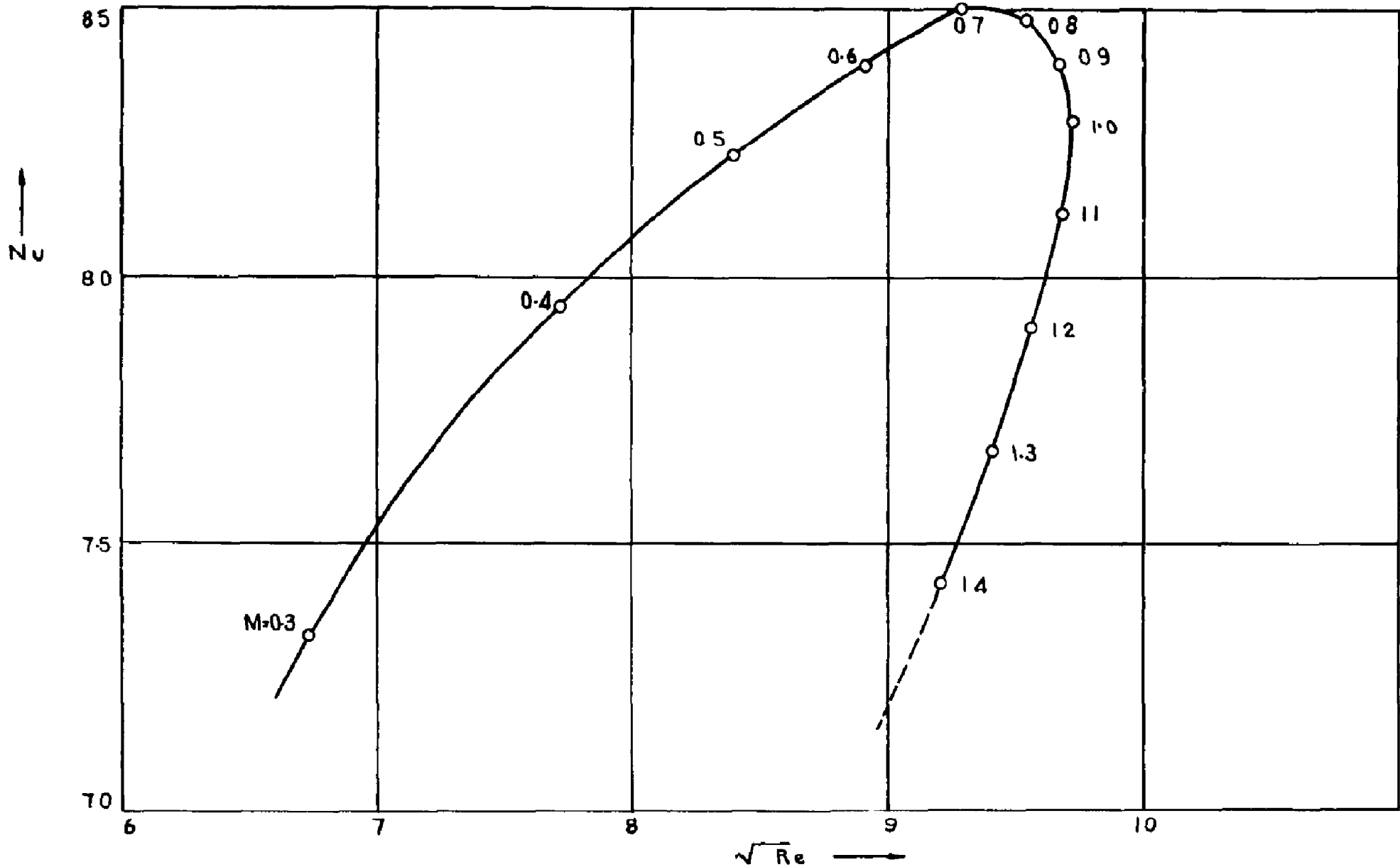
The Nusselt Nº — Reynolds Nº relationship for the wire.

FIG.5.

FIG 6
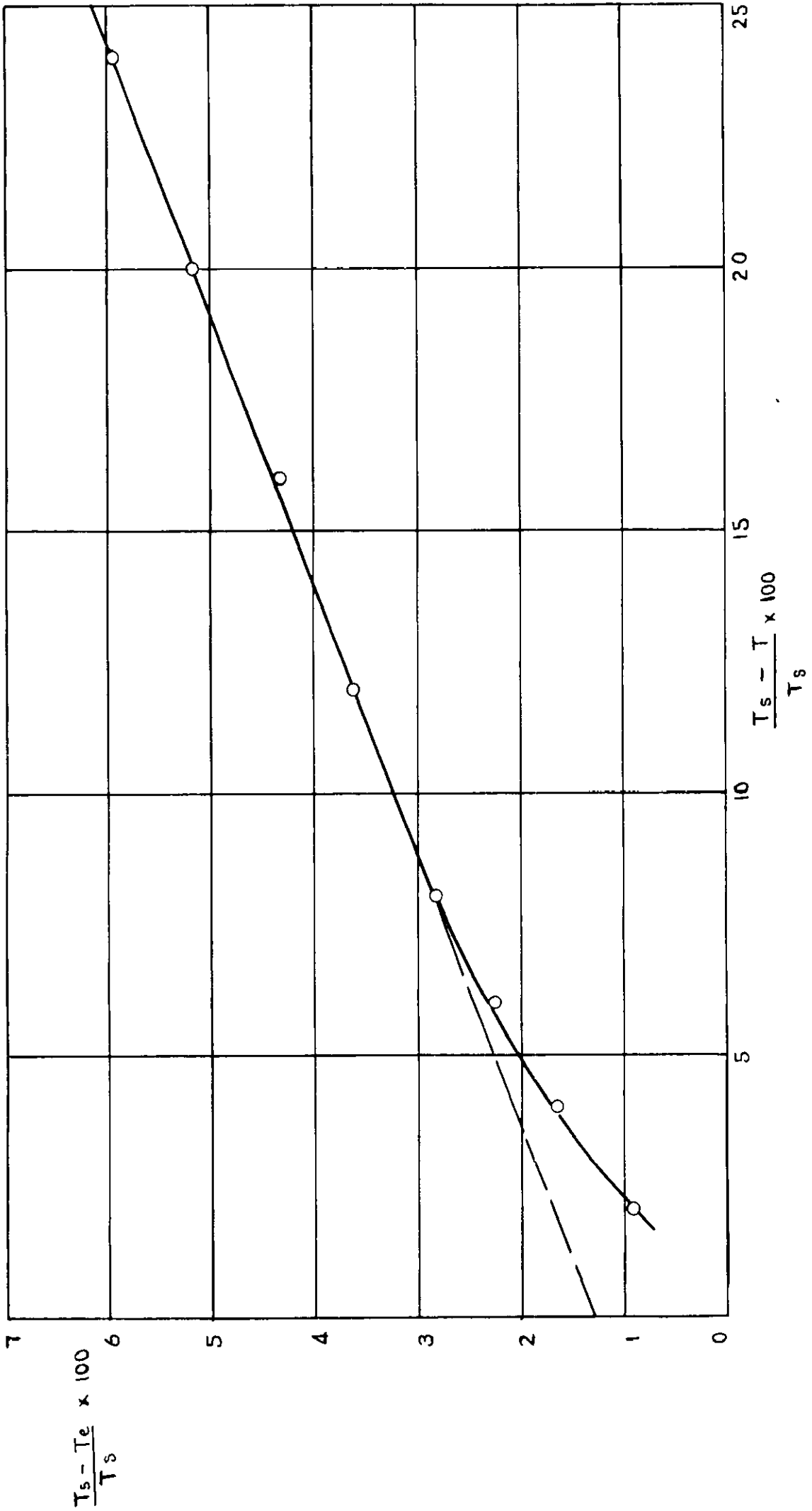
Equilibrium temperature and static temperature

FIG. 7

FIG 8(a)

Leads to wire

"Araldite" body

Copper leading edge

Removable wire unit

wire

Dental porcelain supporting needles

Scale Full size

FIG 8(b)

Leads to wire

Moulded "Araldite" body

Wire holder moulded into body

Scale Full size

FIG 8(c)

Lead $\frac{3}{16}$" x $\frac{1}{16}$" copper

Moulded "Araldite" body

Needles extended to avoid body interference
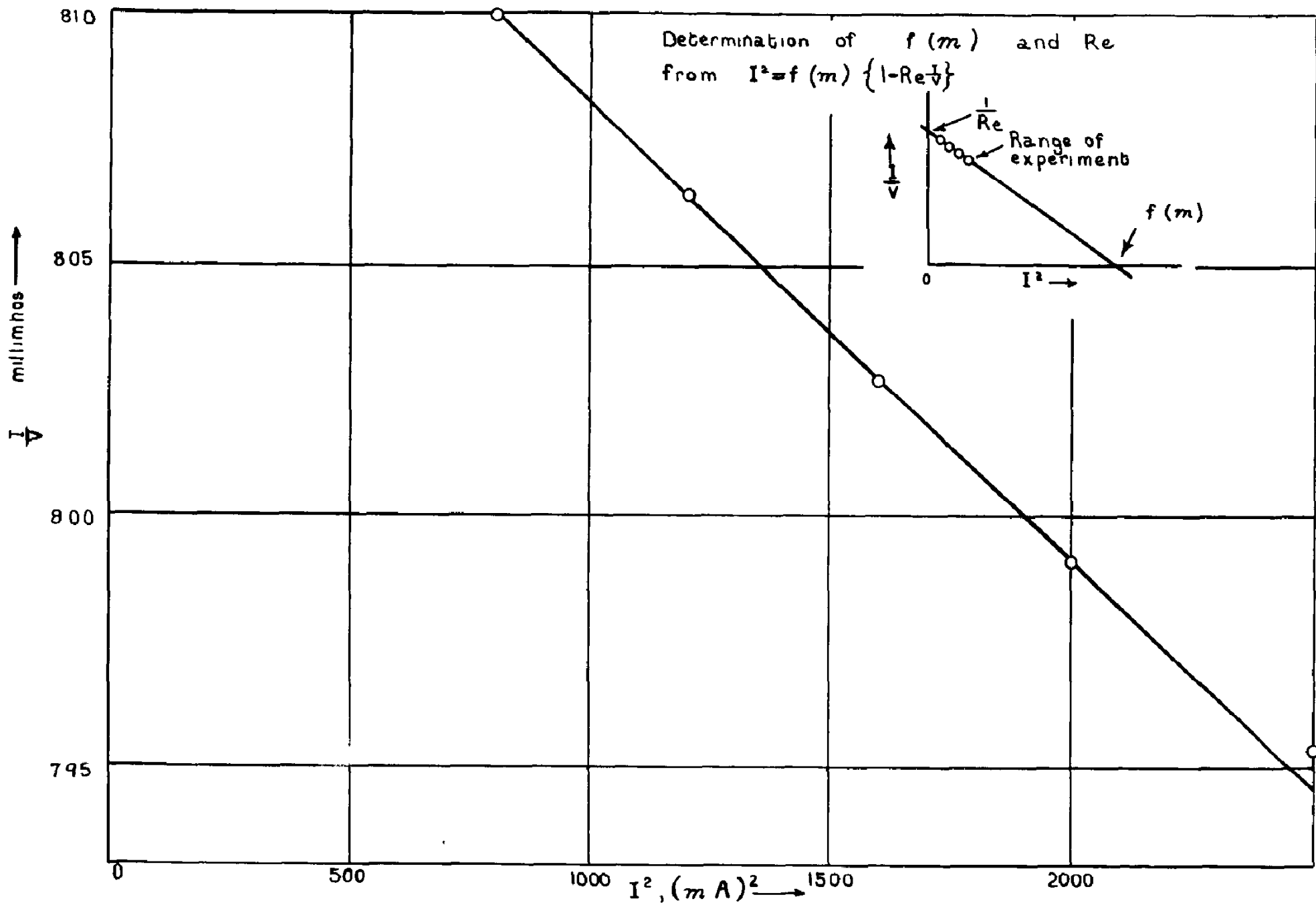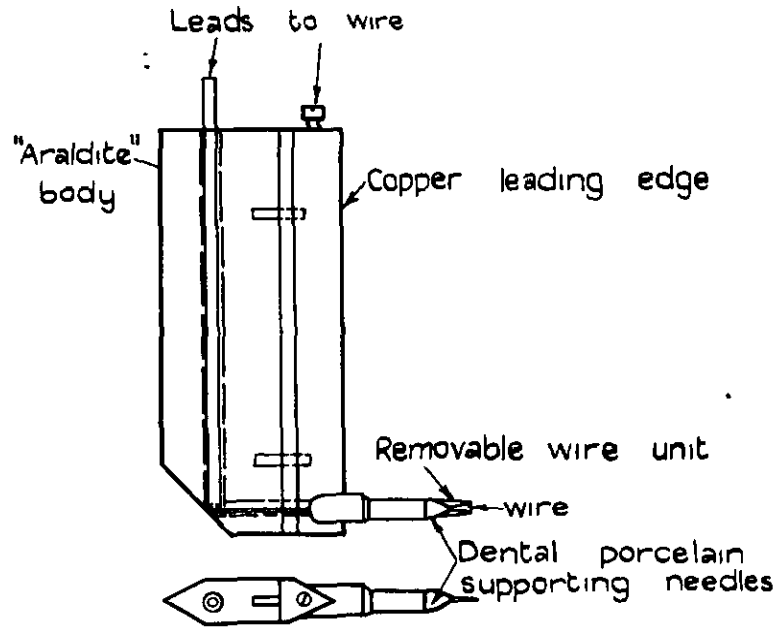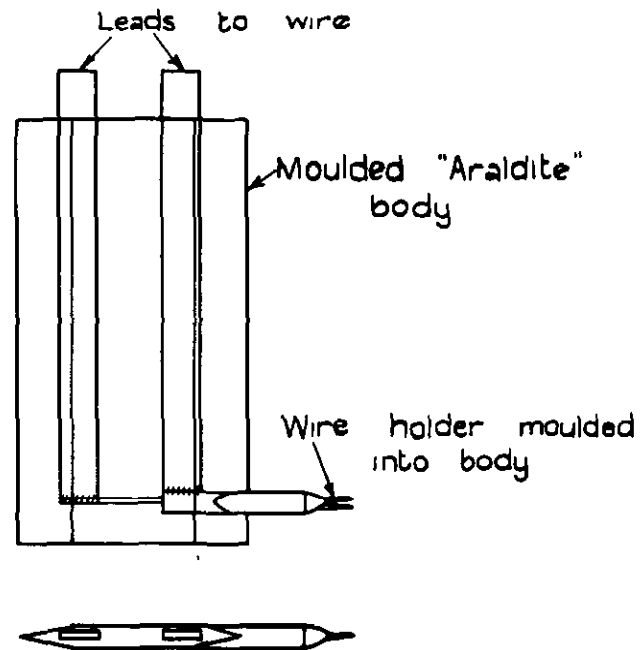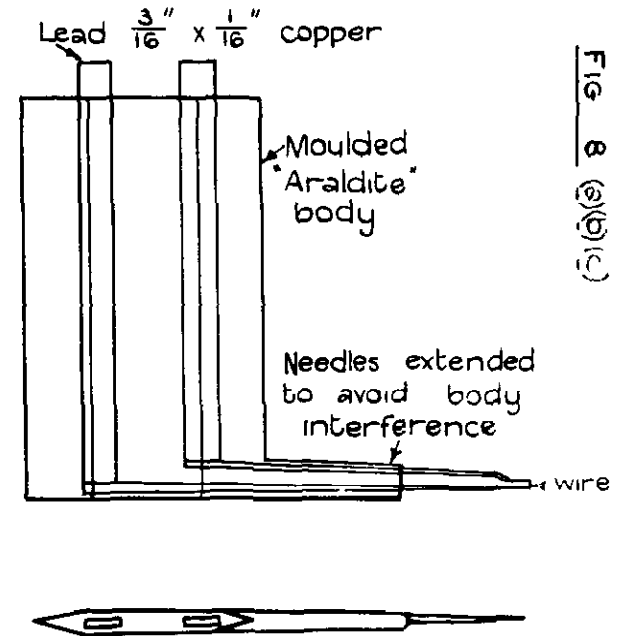
wire

Scale Full scale

FIG 8 (a)(b)(c)

FIG 9
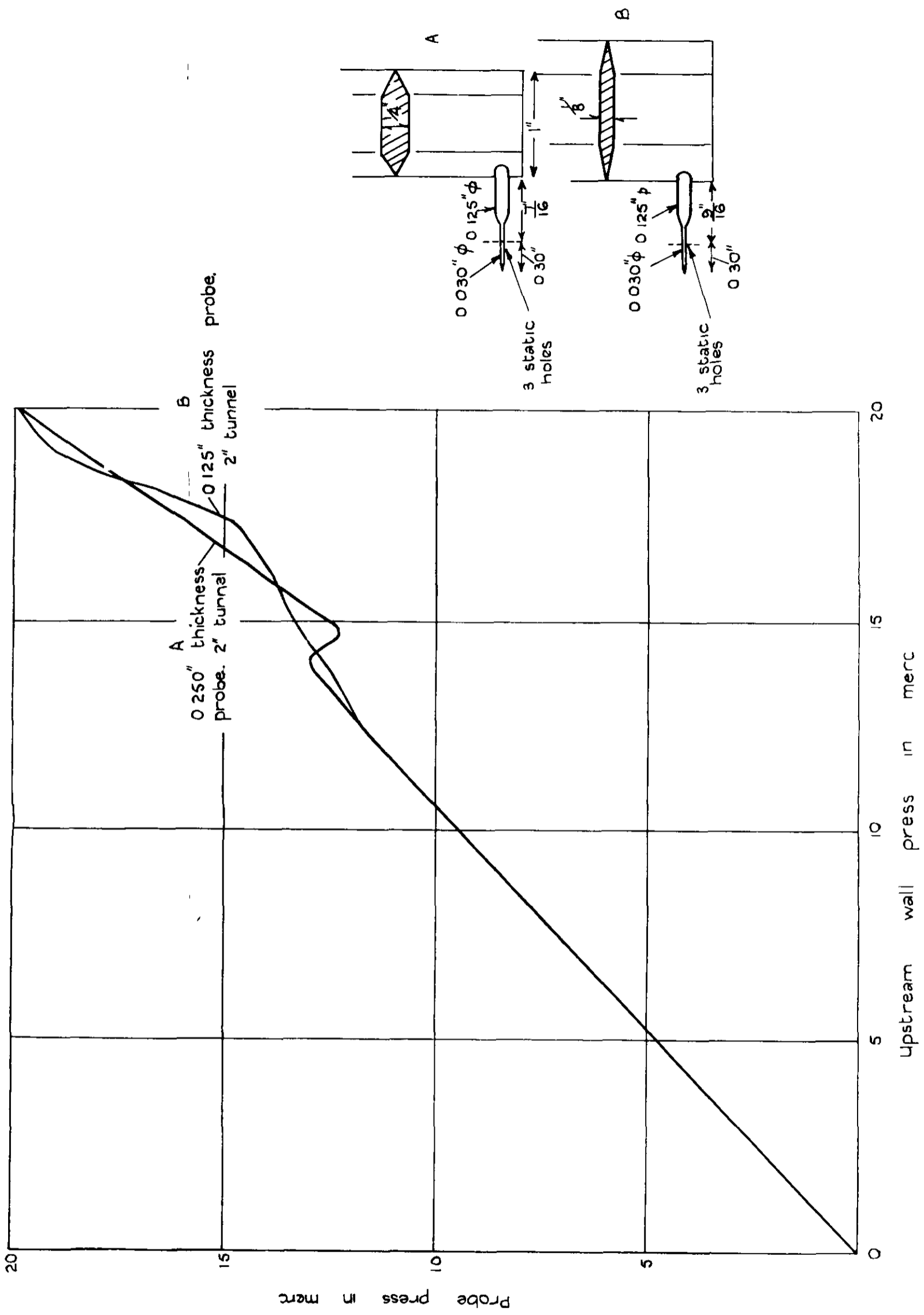
Calbration of hot wire probes
2" tunnel

FIG 10

Probe 'B'
(FIG. 9)
0·125" thick.

Probe 'A' (FIG. 9)
0·250" thick.

Probe press. in merc.

Upstream wall press. in. merc.
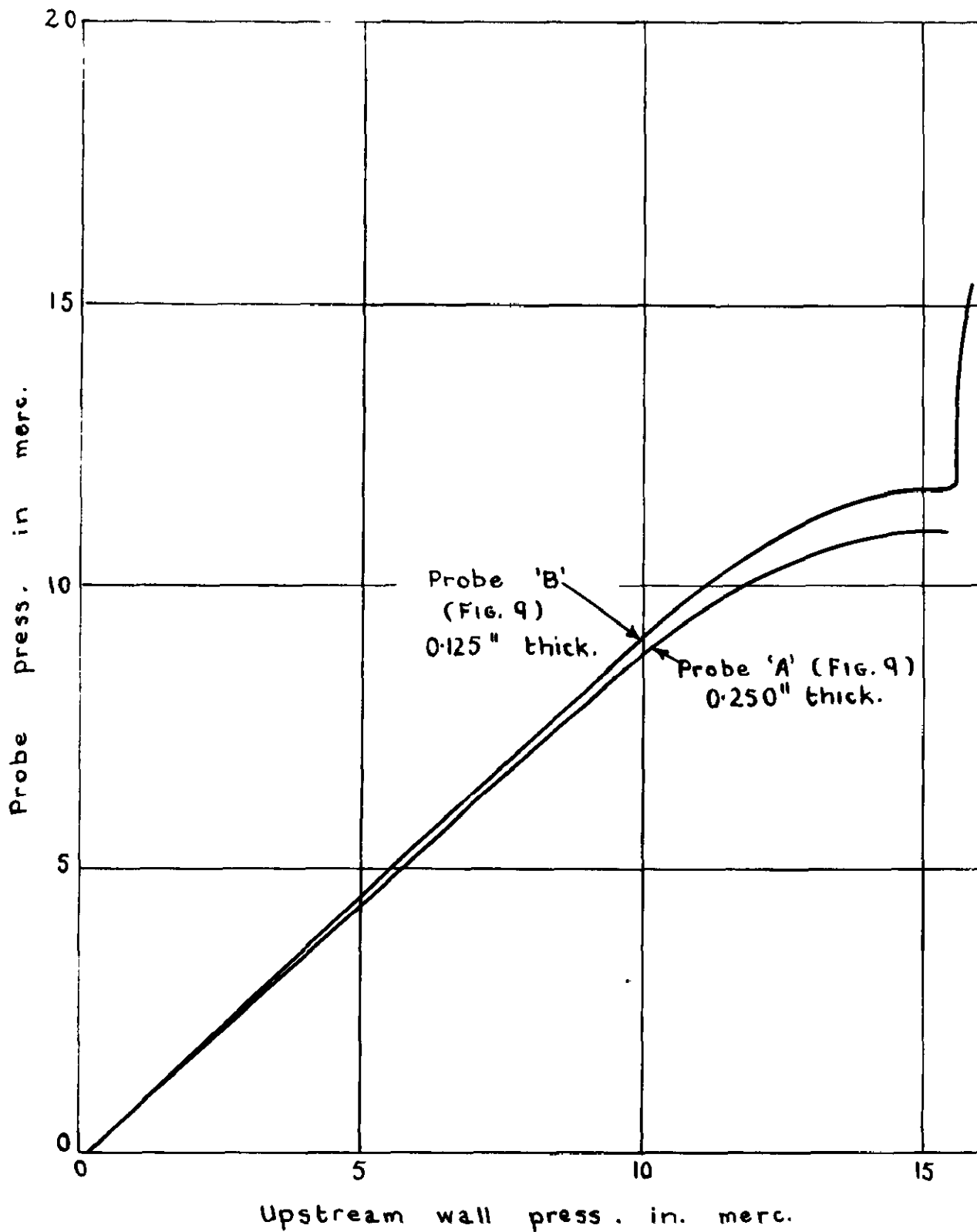
Calibration of hot-wire probes. 9" x 3" tunnel

Calibration of hot-wire probe.
Transonic probe in 9" x 3" tunnel

3 static holes   0.03" ⌀
0.045" ⌀
ogive nose
0.30"
1½"
1 5/16"
⅛"

Probe. Press. In. merc

Upstream wall pressure. In. merc.
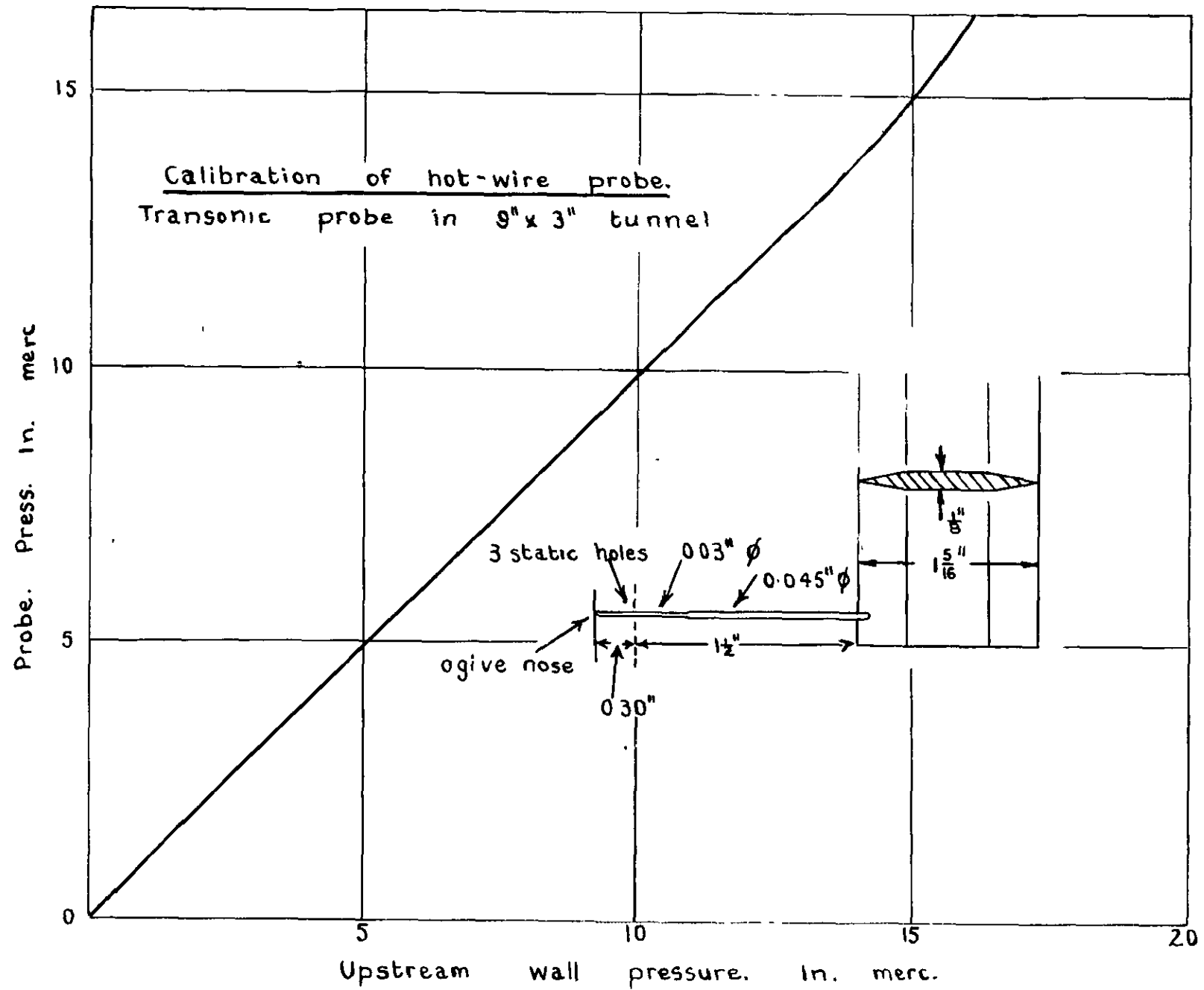
Fig. 11

FIG 12
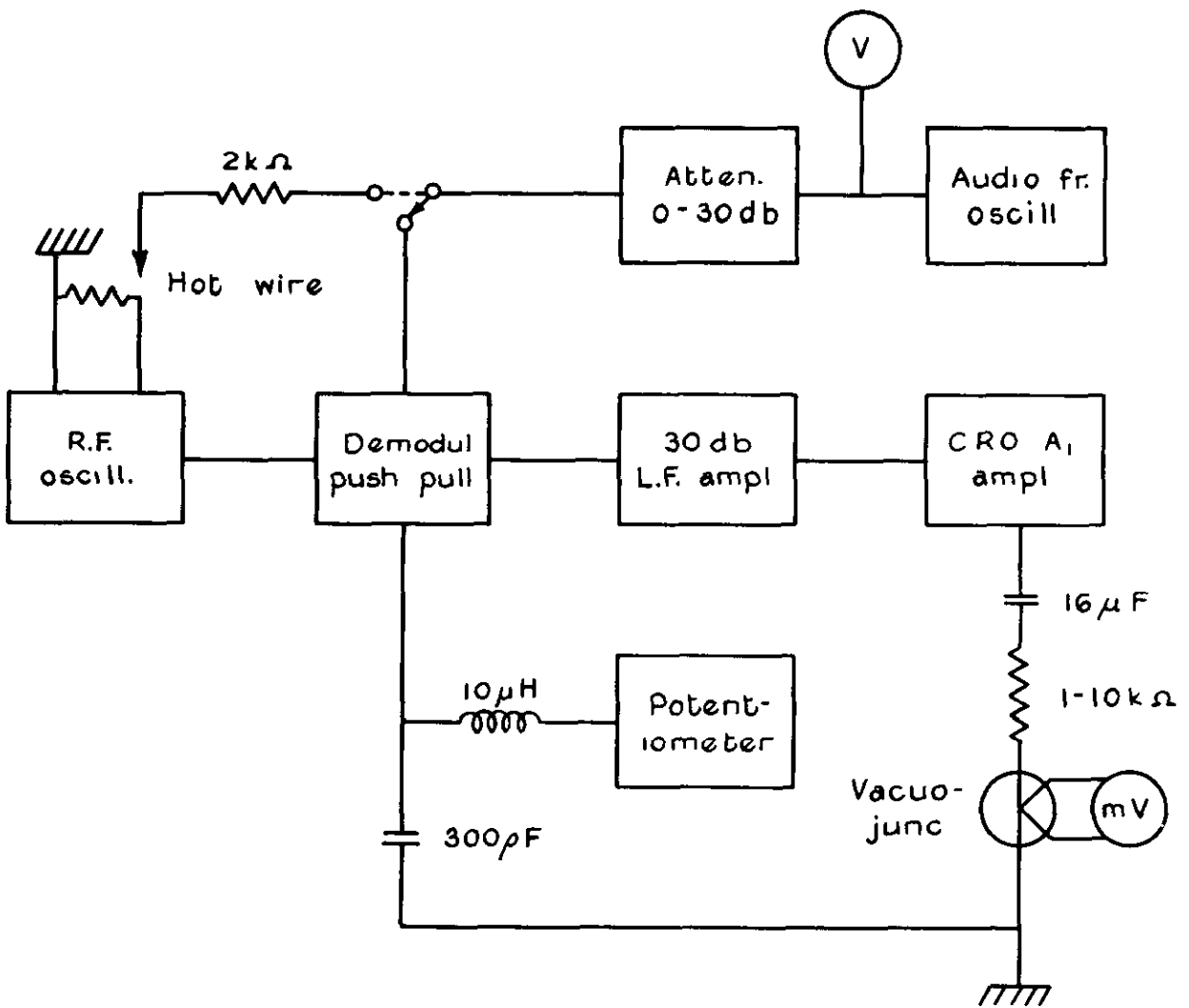
Calibration   of   hot - wire   equipment

FiG 13
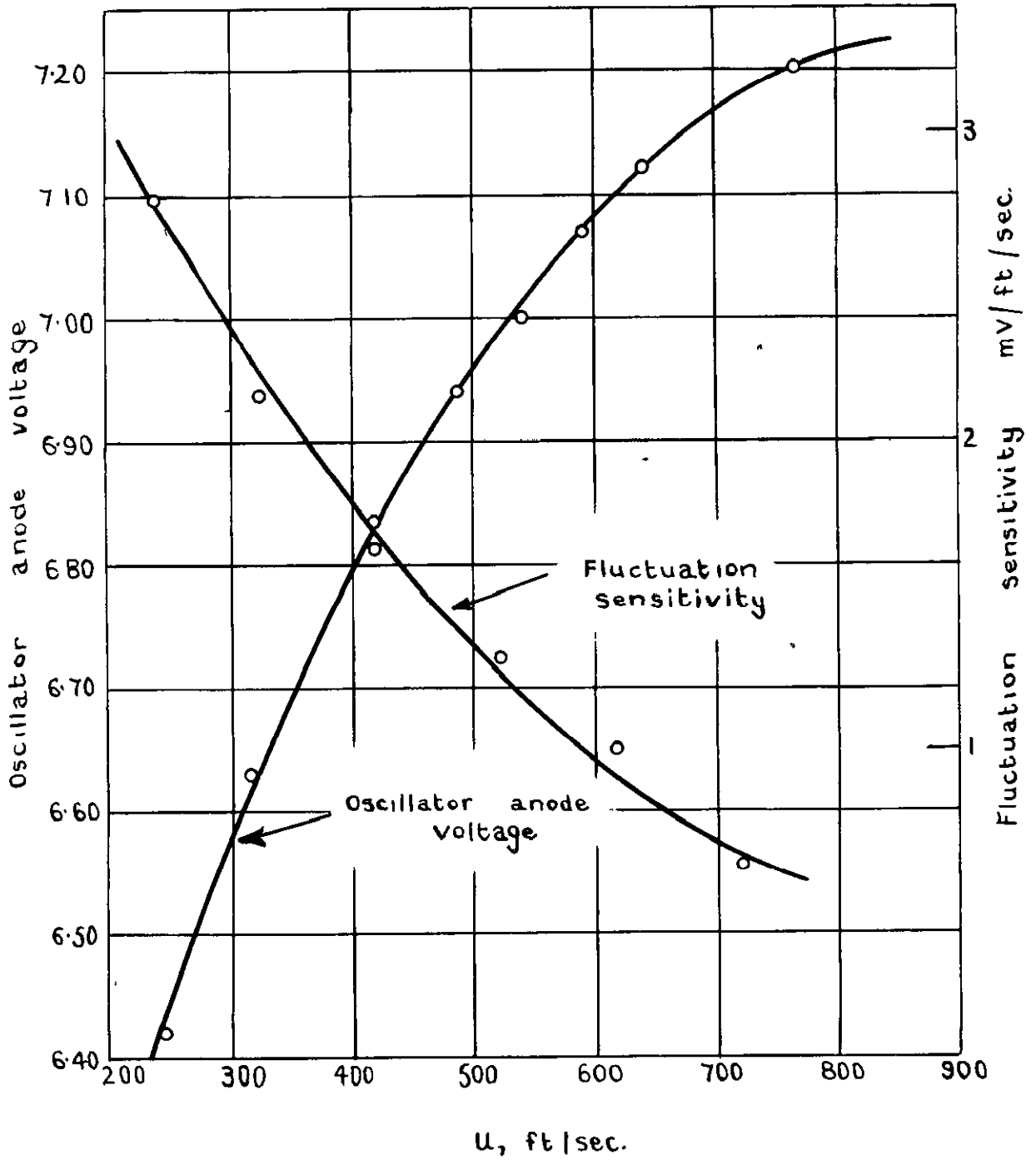
FIG 14
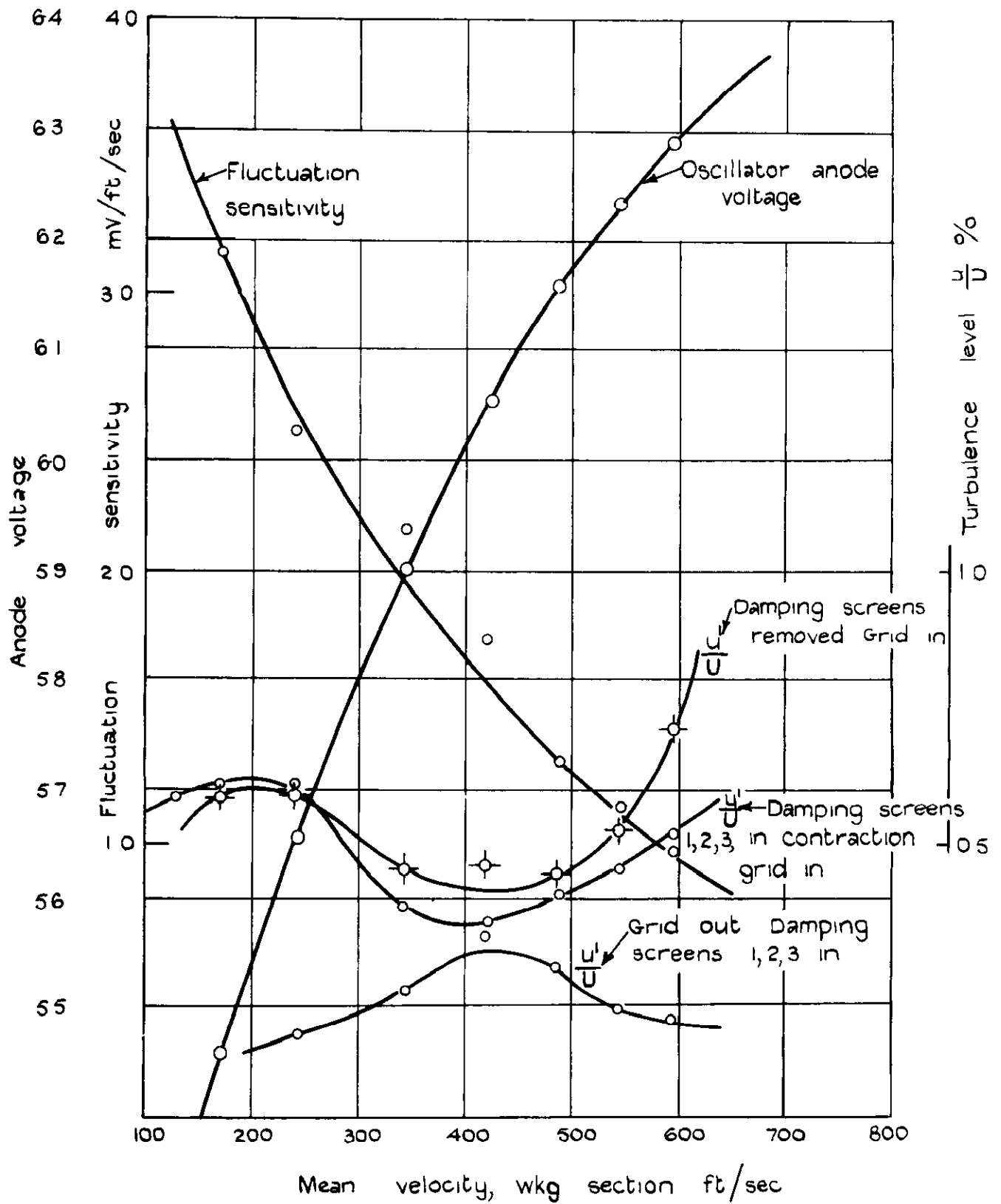
Calibration and turbulence measurements
Transonic liners

FIG 15
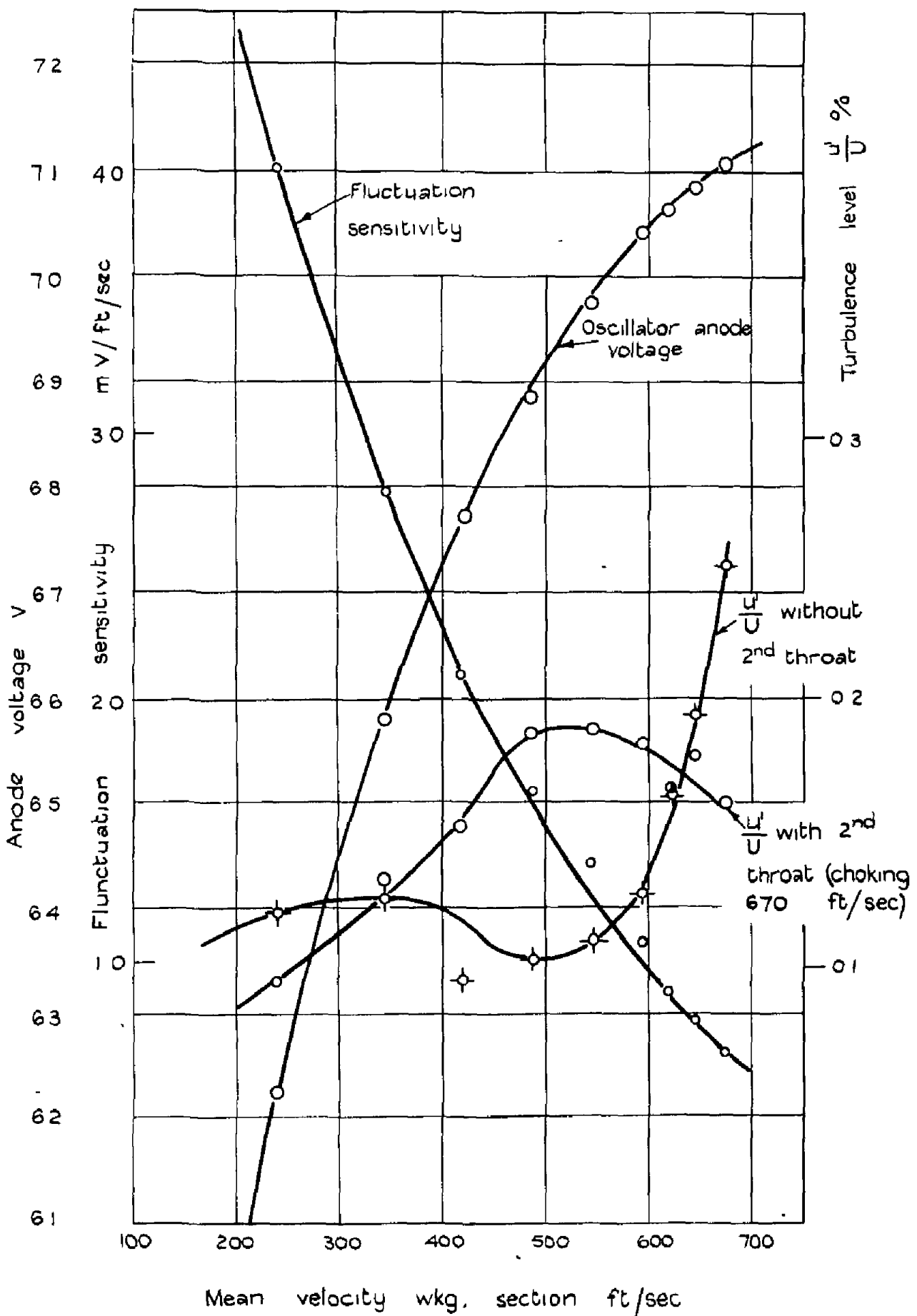
Calibration and turbulence measurements Plane subsonic liners

FIG. 16.

Input ⟶ | High freq. ampl 100c/s -100kc/s | ⟶ | Mixer | ⟶ | Low freq ampl. 0 5 - 20 c/s |

Local oscill. 0-100 kc/s ⟶ Mixer

Mixer ⟶ Cathode Follower ⟶ Vacuo Junc. ⟶ mV

FIG 17

Attenuation dB

20

Input to 1 Output 4 (Normal)

Input to 1 Output 3 4 earthed through 1·8 M Ω

Input

Output

10

1 2 3 4 1·8 MΩ

50 kc/s crystal filter

12 10 8 6 4 2 0 2 4 6 8 10 12

c/s

Off tune centre, freq. = 50kc/s
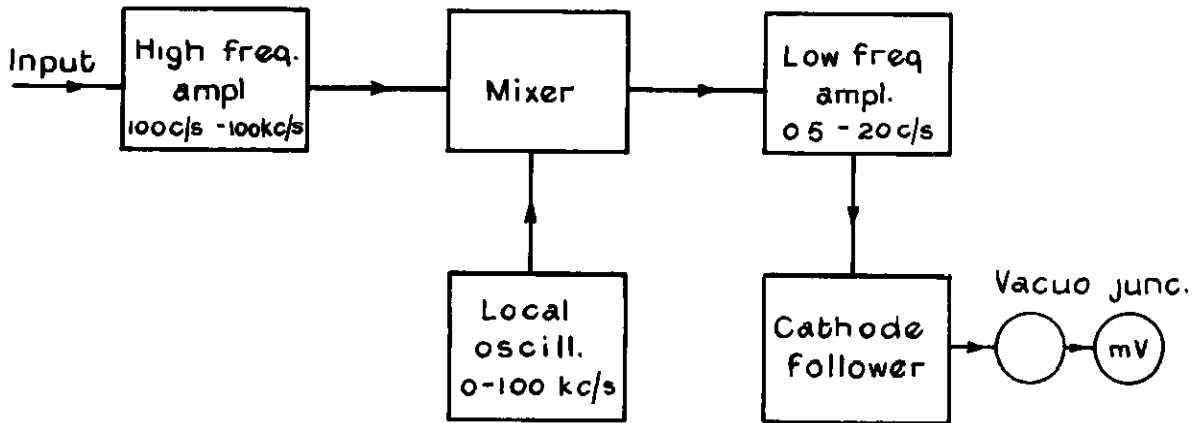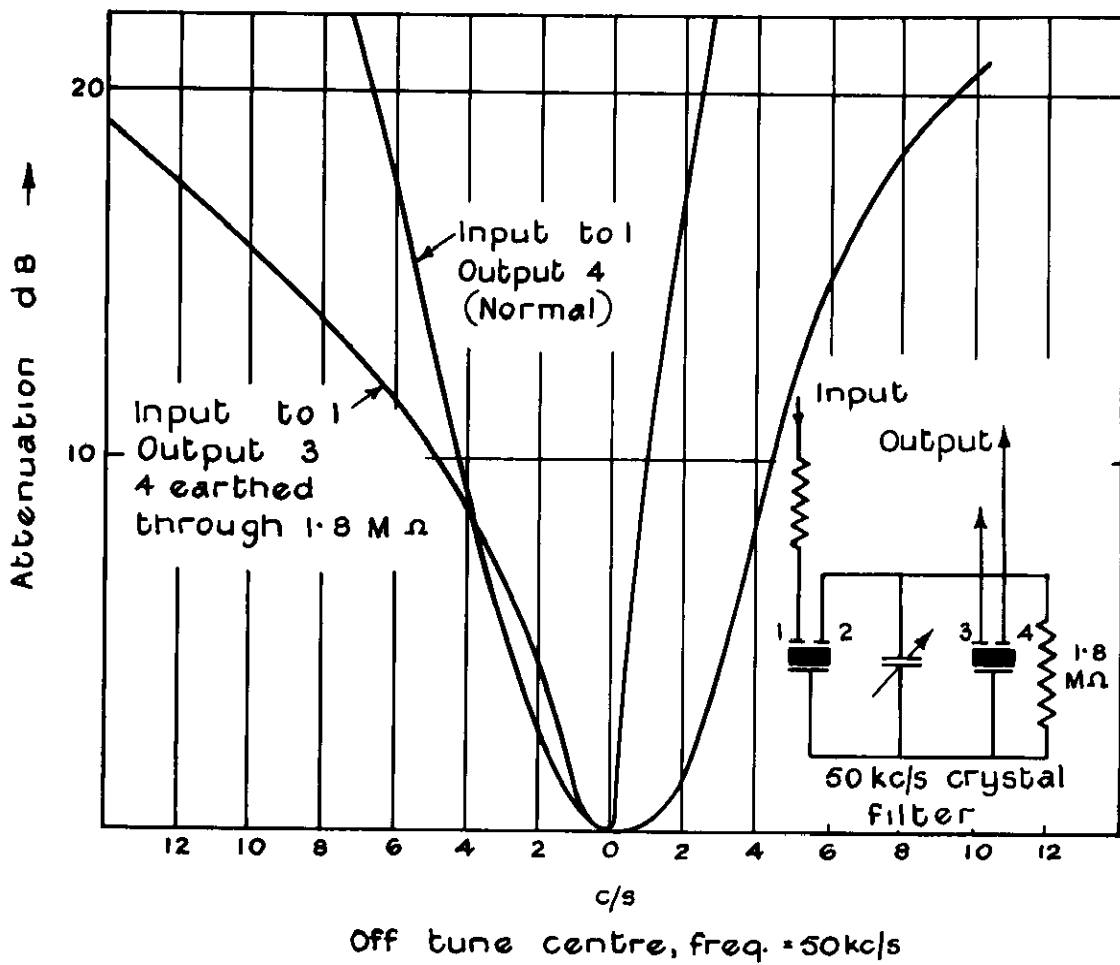
Modifications to crystal filter wave analyser

FIG 18
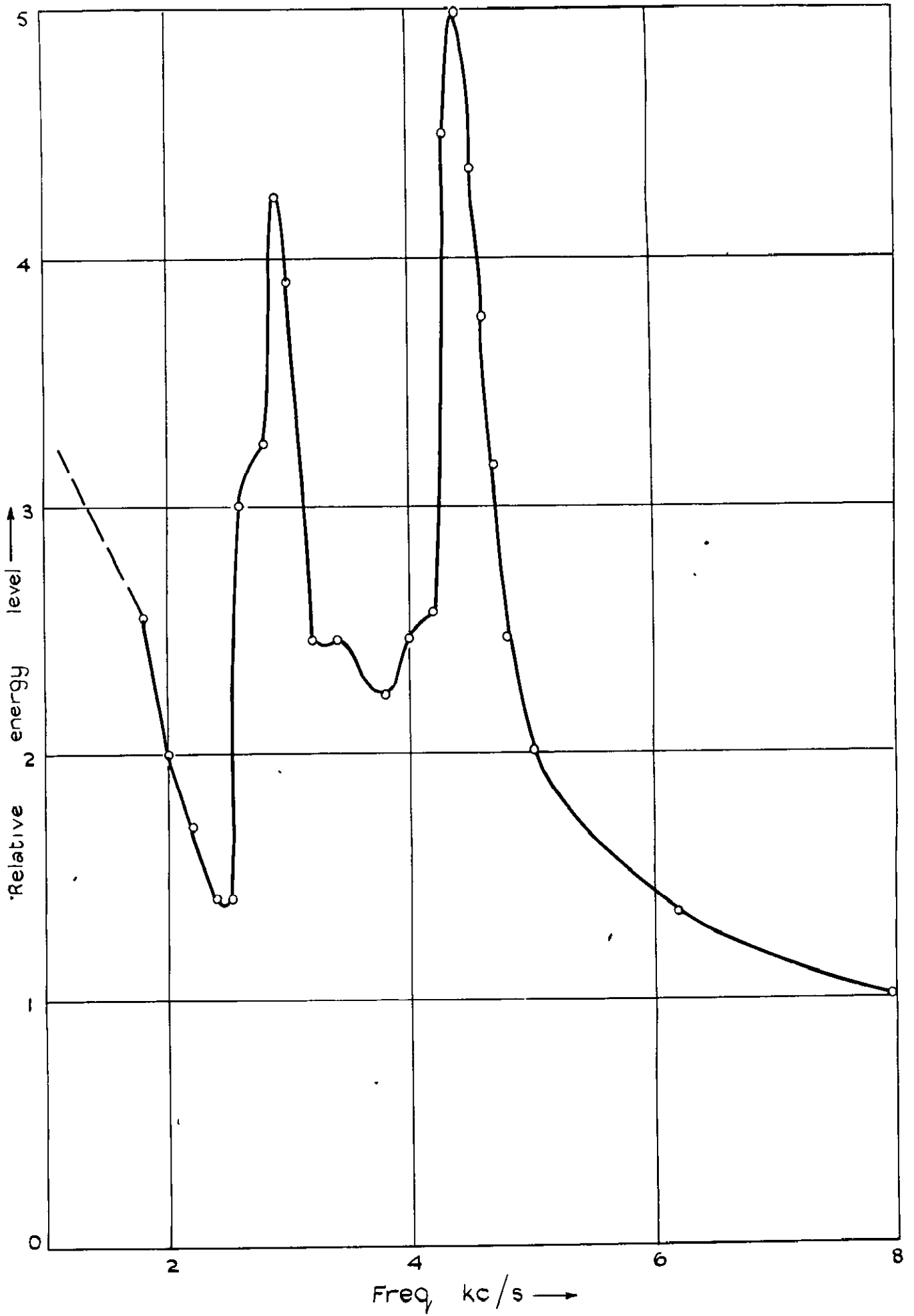
Spectrum in 2" tunnel, M = 0.89
Transonic liners

FIG 19
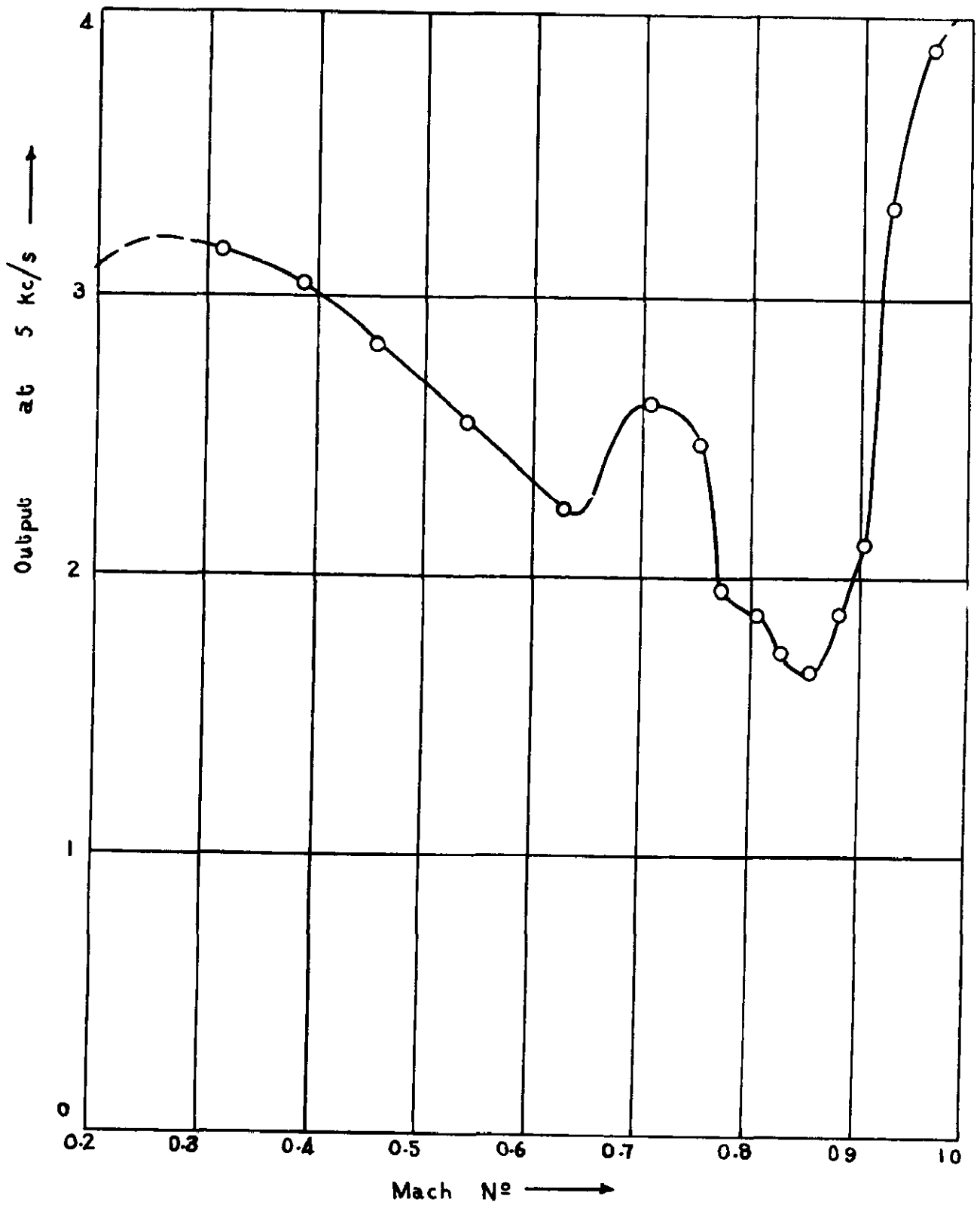
Variation of spectral density with Mach N°.   2" tunnel.

FIG. 20
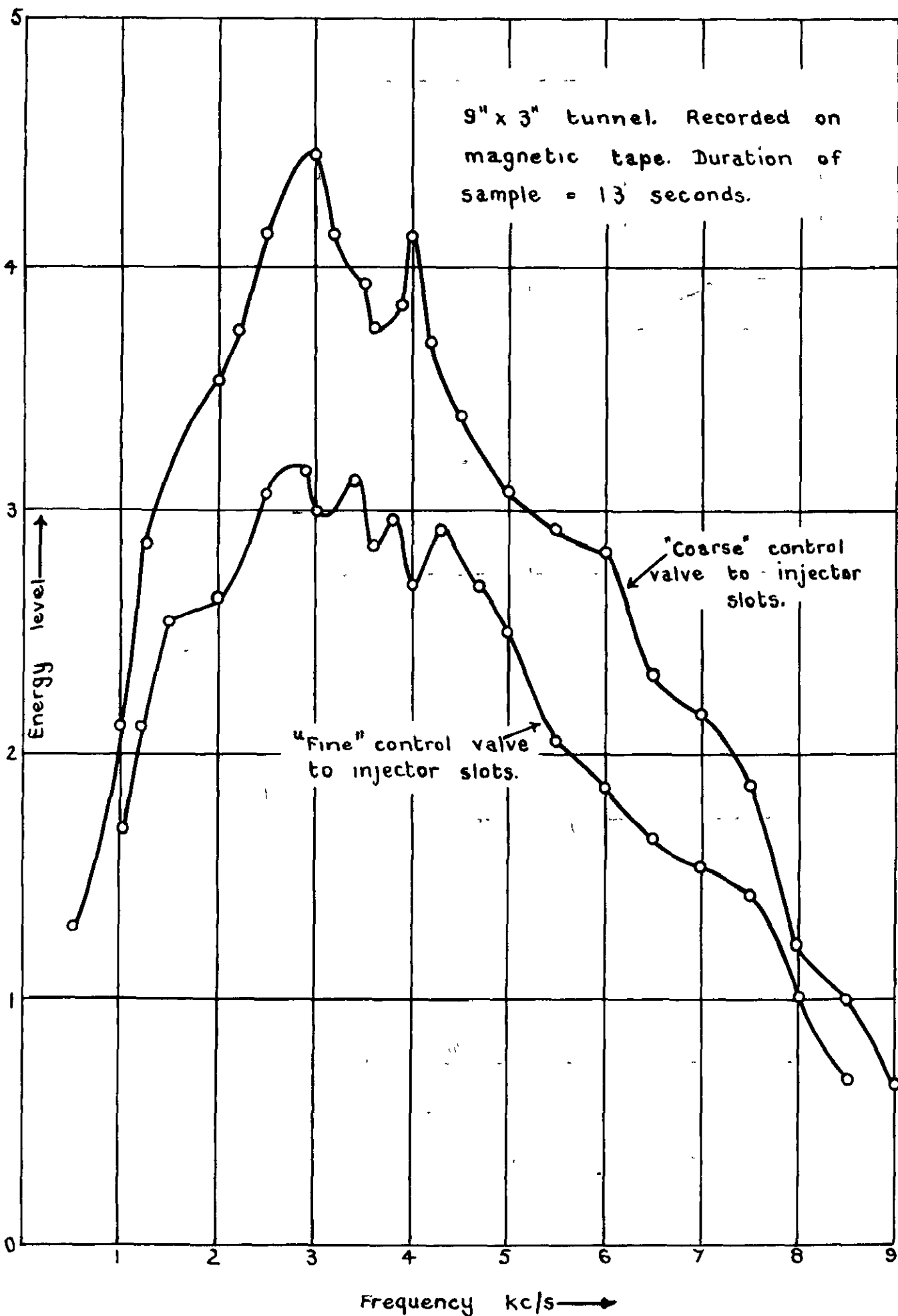
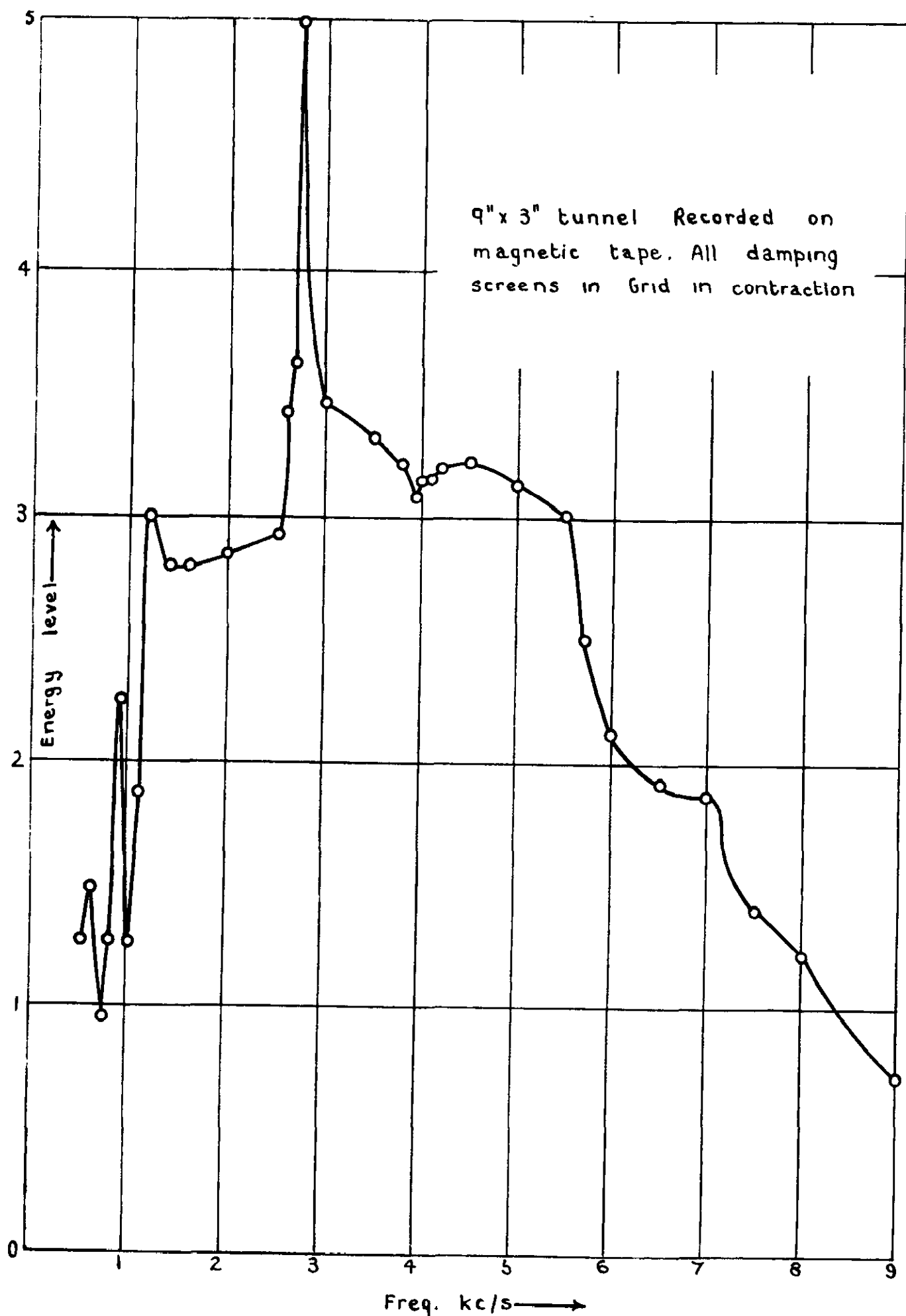Spectrum at M = 0·36 in transonic liners.

FIG 21.
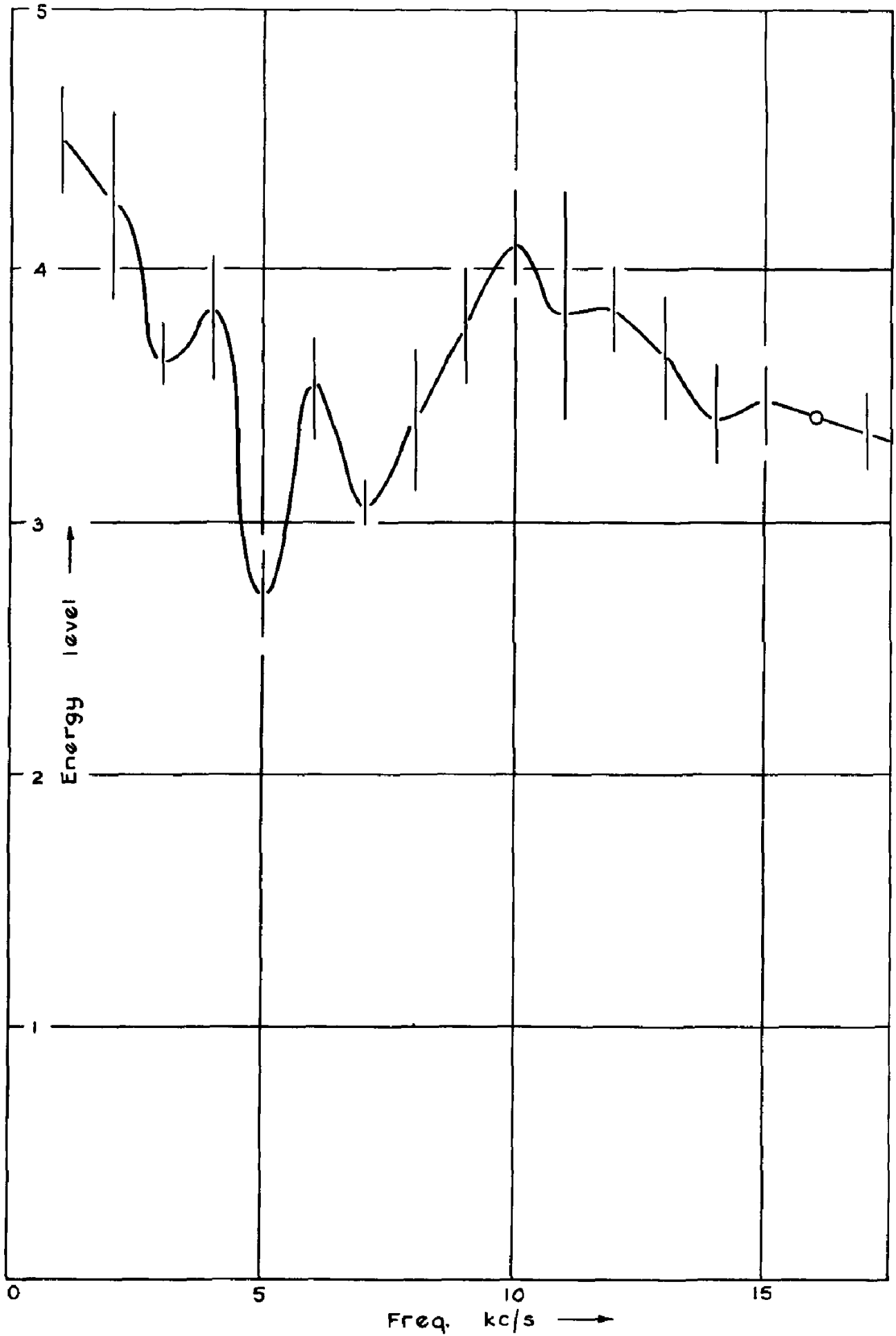
Specimen spectrum with tunnel running. Min^m and max^m during ½ minute intervals at each frequency. M = 0·36. 9" × 3" tunnel. Transonic liners
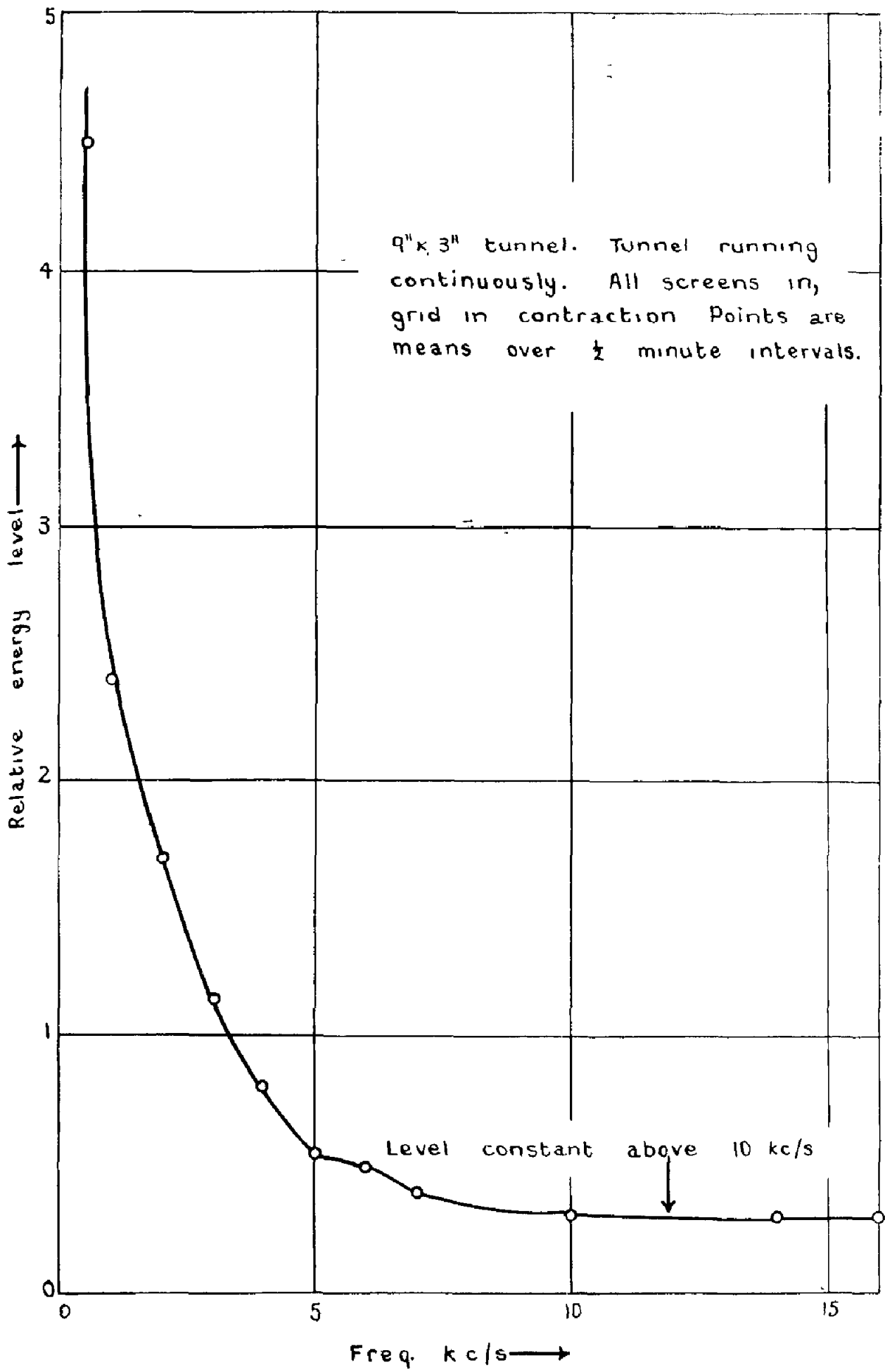
FIG 22
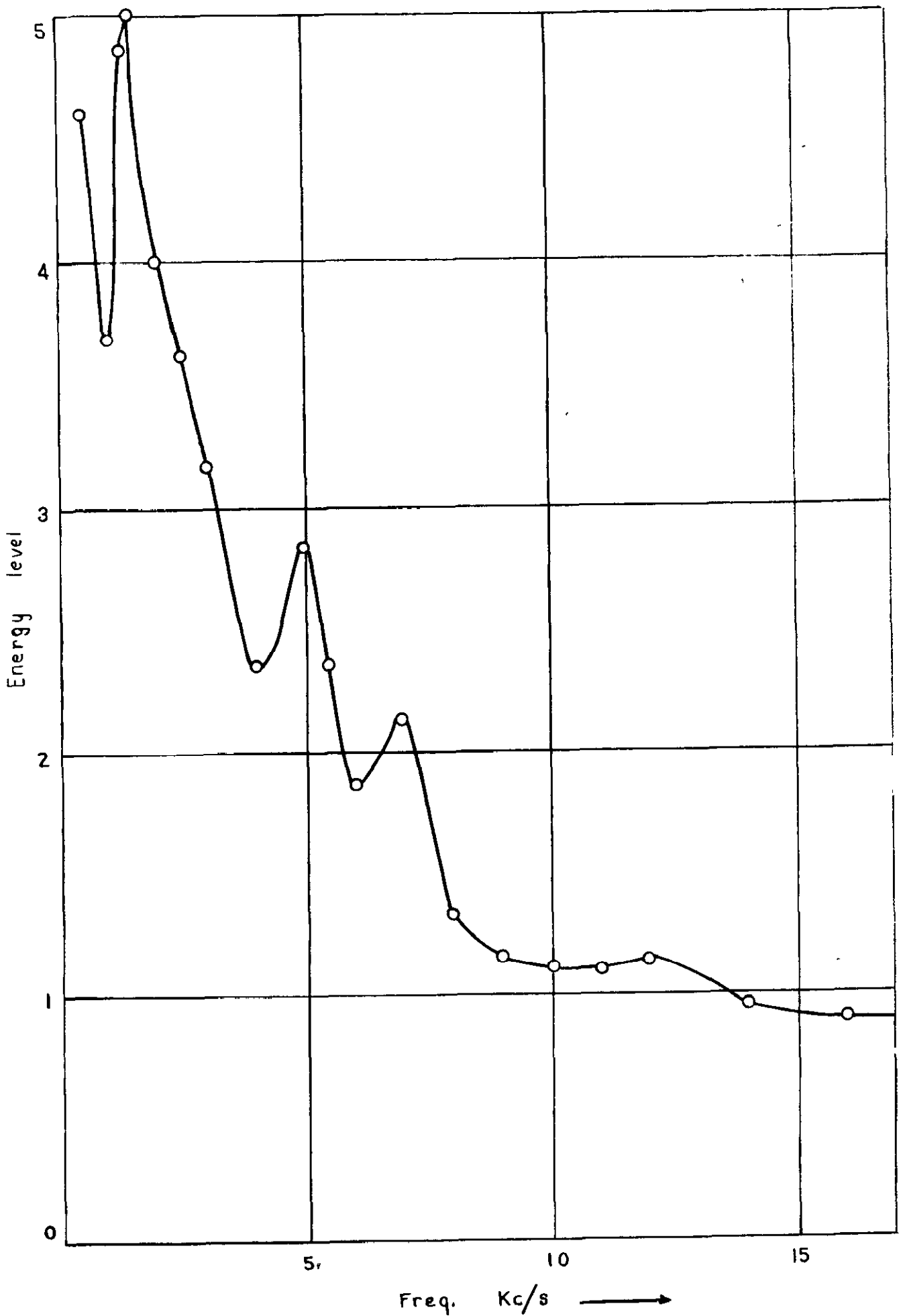
Spectrum in 9"x3" tunnel at M = 0 99. Grid in contraction
Wire 17" from rear of test section, Transonic liners

FIG. 23

9"x 3" tunnel Recorded on magnetic tape. All damping screens in Grid in contraction

Energy level →

Freq. kc/s →

Spectrum at M = 1·8 in free stream.

FIG 24

9" x 3" tunnel. Tunnel running
continuously. All screens in,
grid in contraction Points are
means over ½ minute intervals.

Level constant above 10 kc/s

Relative energy level

Freq. kc/s

Spectrum in free stream at M = 1 80.